Politecnico di Milano

Facoltà di Ingegneria dei Processi Industriali

Degree in Materials Engineering

A Characterization of Nanohole Grating Refractive Index Sensors for Biosensing Applications

A Thesis Submitted to the Faculty of
Politecnico di Milano by
Alyssa Bellingham

Matricola: 781868

Advisor Dr. Carlos Angulo Barrios
Universidad Politécnica de Madrid, Madrid, España
Co-Advisor Dr. Adam Fontecchio
Drexel University, Philadelphia, Pennsylvania, United States of America
Co-Advisor Dr. Maria Cristina Tanzi
Politecnico di Milano, Milano, Italia

Academic Year 2011-2012

For the wonderful friends I have made during my travels

Contents

List of Figures

Acknowledgements

I would like to start by thanking my parents Kathleen and Jeffrey Bellingham for their unwavering support, trust, and encouragement in me and my dreams. I thank my sister, Kate, for always being able to make me laugh and my brother, John, for allowing me to think I might have had some influence on his decision to become an engineer. I would like to thank Paul for always supporting me and being extremely patient with my short temper and busy schedule. I thank my grandparents for inspiring me to reach outside my horizons and explore the world.

I would like to acknowledge my research advisor at Drexel University, Dr. Adam Fontecchio, for his all his support and advice over the past five years. Dr. Fontecchio and Drexel University have provided me many opportunities above those typically available to students, including the opportunity to complete the work for this Master's degree in America, Italy and Spain as part of the EAGLES program. My research advisor's unwavering support and trust in me is what has allowed me to pursue my research interests, forge international collaborations, and attend local and international conferences. Without his support, I would not be completing this degree and continuing my education as an National Science Foundation Graduate Research Fellow at Drexel University in the upcoming year.

I would like to thank my research advisor at Universidad Politecnica de Madrid(UPM), Dr. Ing. Carlos Angulo Barrios, for welcoming me into his lab to complete the research for this project. He was always available for discussion and took an active interest in the project. His support, advice and feedback have been invaluable during this project.

I would also like to thank Vctor Canalejas Tejero for all his help and advice on this project. He taught me everything I needed to know about the fabrication and characterization equipment in the lab, fabricated all the gratings for this project, and provided helpful insight and feedback on my work. I

would never have been able to complete this project without all of his help. I would also like to acknowledge Sonia Harranz and Sergio Carrasco for all their help with the chemistry aspects of the project. They have been invaluable in preparing the recognition elements(MIP and biomolecules)for this project. Gracias!

I would like to thank the members of my committee from Politecnico de Milano, Dr. Maria Cristina Tanzi, and Dr. Marco Ormelese for their feedback on my thesis. I really value their insight and appreciate the feedback.

I would also like to thank all my colleagues in the Drexel Nanophotonics lab in Philadelphia, USA, who have supported me in my research career through discussion and joint project work including Dr.Kashma Rai, Dr. Sameet Shriyan, Mr. Jared Coyle, Mr. Ben Pelleg, Ms. Elizabeth Plowman, Ms. Yang Gao, and Ms. Sylvia Herbert. I would also like to acknowledge all my other labmates who have provided a friendly and supportive research environment including Dr. Anna Fox, Dr. David Delaine, Ms. Jamie Kennedy, Mr. Yohan Seepersad, and Mr. Bill Hicks. Tambin me gustara agradecer a todos mis colegas en el laboratorio de la UPM ISOM que me han ayudado en este proyecto y nos hizo mi breve tiempo en Espaa muy agradable. Grazie a tutti i miei amici in Italia che mi hanno sostenuto durante questa ricerca.

I would like to acknowledge the Engineers As Global Leaders for Energy Sustainability (EAGLES) program and all the people involved for providing me with the opportunity to complete this degree across three countries. I would especially like to thank Marcia Henisz, Holly Burnside, Amy Campbell, and Michela Gregori for all their support and help during this program.

Last but certainly not least, I thank Dr. Selcuk Gucieri for mentoring and supporting me since the first day I met him while visiting Drexel on a college visit. He has provided me with more opportunities than I can count and has always encouraged me to pursue my research and academic interests.

Abstract

Sub-wavelength periodic structures imprinted in metallic films give rise to enhanced transmission features which are sensitive to changes in refractive index at the surface. Variations in the transmission spectral output can be quantified to detect the concentration of analyte in a solution and the surface of the film can be readily modified with a variety of synthetic recognition elements, biomolecules, and well-established silane chemistry to allow for molecule recognition at the surface of the grating. These nanohole gratings can also be used to couple light into planar optical waveguides, which make ideal signal transducers because of their sturdiness, easy patterning of reagents, and easy incorporation of polymer materials. This thesis seeks to characterize nanohole structures imprinted on aluminum thin films as refractive index sensors that can be incorporated as transduction elements into biosensing technologies as well as to provide a path to optimization of an integrated biosensing device.

Aluminum, a previously unexamined material for these nanohole array imprinted devices, was used as the metallic thin film in this thesis. The material demonstrated similar enhanced transmission effects to well known plasmonic materials like silver and gold, which cost significantly more than aluminum. The aluminum film was imprinted with a periodic nanoscale array of holes using an etching procedure, and then evaluated as a refractive index sensor. The bulk sensitivity of the nanohole array samples was determined through solvent characterization as well as exposure to varying thicknesses of a deposited layer of polymer. The ability of the potential transduction element to detect affinity reactions occurring at the surface was evaluated using well known biomolecular recognition experiments as well as synthetic recognition experiments using molecularly imprinted polymer films (MIPs).

MIPs are biomimetic recegnition elements that can be created for a variety of molecular structures, enable large-scale chip fabrication, are reusable, and offer superior stability when exposed to solvents and temperature extremes.

The potential to combine the nanohole array transducer element with this synthetic recognition element is examined in this thesis. A theoretical optimization of the grating pitch for optimal detection capability was performed and the future path of optimizing an integrated biosensing device is discussed.

Estratto in lingua italiana

Le strutture periodiche di lunghezza donda inferiore impresse in film metallici danno origine a caratteristiche migliorate di trasmissione che sono sensibili alle variazioni dell'indice di rifrazione sulla superficie. Le variazioni nellemissione spettrale possono essere quantificate per rilevare la concentrazione di analita in una soluzione e la superficie del film pu essere facilmente modificata con una variet di elementi di riconoscimento sintetici, biomolecole e applicando la ben consolidata chimica del silano al fine di consentire il riconoscimento della molecola alla superficie della griglia. Questi reticoli nanohole possono essere utilizzati anche per indirizzare la luce in guide donda ottiche piane, il che li rende trasduttori di segnale ideali a causa della loro robustezza, della facile schematizzazione dei reagenti, e della facile integrabilit con materiali polimerici. Questa tesi cerca di caratterizzare strutture nanohole impresse su film sottili di alluminio come sensori di indice di rifrazione che possono essere incorporati come elementi di trasduzione in tecnologie di biopercezione e per fornire un percorso di ottimizzazione di un dispositivo integrato di biosensori.

Alluminio, un materiale precedentemente inesplorato per questi dispositivi di matrice nanohole impressa, stato utilizzato come film metallico sottile e ha dimostrato effetti similari a ben noti materiali plasmonici come l'argento e l'oro, che costano molto di pi rispetto all'alluminio, nel miglioramento nella trasmissione,. Il film di alluminio stato stampato con un ordinamento nanometrico periodico di fori utilizzando una procedura di incisione, e quindi valutato come un sensore di indice di rifrazione. La sensibilit bulk dei campioni di matrice nanohole stata determinata attraverso la caratterizzazione del solvente cos come attraverso l'esposizione a diversi spessori di uno strato di polimero depositato. La capacit dell'elemento di trasduzione di rilevare reazioni di affinit che si verificano in corrispondenza della superficie stata valutata utilizzando ben noti esperimenti di riconoscimento biomolecolare nonch esperimenti di riconoscimento sintetico usando dei molecularly impressed polymer films (MIP).

I MIP sono recettori biomimetici che possono creare recettori per una variet di strutture molecolari, abilitare la fabbricazione di chip su larga scala, sono riutilizzabili, e offrono una stabilit superiore quando esposti a solventi e a temperature estreme. La potenzialit di combinare lelemento trasduttore a struttura nanohole con lelemento di riconoscimento sintetico viene qui esaminata. Una ottimizzazione teorica del passo di griglia per la capacit di rilevazione ottimale stata eseguita e il percorso futuro di ottimizzare un dispositivo integrato di biorilevamento discusso.

Chapter 1

Introduction

1.1 Motivation

There is a great need for powerful analytical and diagnostic tools in biomedical industries for identifying diseases, monitoring biomolecular interactions, and improving diagnostic tests. Compact devices integrating biological or biologically derived recognition elements with physiochemical transducers, or biosensors, provide a means of achieving such tools. Biosensors are able to rapidly detect trace quantities of biomolecules such as viruses,[1] drugs,[2] airbourne and waterbourne pathogens,[3] and lipid bilayers.[4] In the past 20 years, biosensors have also become an established method of measuring molecular interactions. However, biosensing technology is still limited by many factors including, cost, efficiency, manufacturing procedures, speed, and sensitivity. These limitations arise from the individual biosensor components as well as their interaction with each other.

Plasmonic materials, such as gold and silver, can support surface electromagnetic oscillations, known as surface plasmon polaritons (SPPs). Theses SPPs be excited by incident light in a resonant manner giving rise to surface plasmon resonances (SPRs) that are sensitive to changes in the dielectric material in contact with the surface.[5] Such SPR transducers are capable of characterizing molecular binding reactions in real-time without the need for additional labeled molecules to assist in the detection process. The most commonly used SPR set up is present applications is the Kretschmann configuration. In this configuration an evanescent field created at the point of total internal reflection in a prism penetrates through a metallic film on the bottom of the prism giving rise to SPRs at the opposite side. However, this setup requires the use of prisms to excite SPPs, which can be bulky and dif-

ficult to integrate into biosensing devices. Sub-wavelength periodic structures fabricated on metallic thin films, also known as nanohole arrays, present an alternative sensing scheme that allows for miniaturization, collinear optical detection for easy integration into biosensors, and multiplexing.[6] Nanohole arrays exhibit unexpectedly high transmission due to the coupling of incident light with SPRs through the holes at the surface of the metallic film.

An optical transducer elemnt made of a sub-wavelength periodic structure imprinted on a metallic thin film, henceforth referred to as nanohole gratings or arrays, presents several advantages over existing biosensing technologies including, stability in a range of solvents, low cost, easy production, and high sensitivity. Much SPR sensing research over the past few years have been directed towards optimizing nanohole arrays fabricated in well know plasmonic materials like gold[6,7] and silver,[4,8] which have demonstrated nearly equivalent sensitivity to existing SPR sensing transducers using the Kretschmann configuration. Despite the many advantages of the nanohole array configuration, this technology has yet to take hold of the SPR transducer market due to the cost limitations imposed by the plasmonic materials. This thesis seeks to achieve equivalent sensitivity to leading SPR transducers using aluminum as the plasmonic material.

Additionally, the use of biomolecule recognition elements imposes environmental and cost restrictions on biosensors. Biomimetic recognition elements, which mimic the geometry and specificity of actual biomolecules, can greatly increase the stability and lower the cost of the device while maintaining equivalent selectivity. Molecularly imprinted polymer (MIP) shows great promise as a highly selective, cheap, and easy to fabricate biomimetic recognition element. This material was combined with the nanohole array transducer in this thesis to demonstrate the potential benefits of an integrated device.

1.2 Contribution

The primary contribution of this thesis is to provide a path to the optimization of a cheaper metallic sub-wavelength periodic array transducer incorporating molecularly imprinted polymer(MIP) technology as the recognition element. Detection of refractive index changes at the surface of the nanohole array was accomplished through surface plasmon resonance (SPR) sensing indicating that the metallic thin film material must be a plasmonic material. Aluminum was examined as the metallic thin film material to provide a cheaper alterna-

tive to conventional plasmonic materials, such as silver and gold. Reducing the cost of nanohole array SPR transducers would allow them to compete with leading SPR transducers in the biosensor market.

The bulk sensitivity of the transmission of the nanohole array to changes in refractive index at the surface was determined through transmission spectroscopy and compared to that of nanohole arrays fabricated in well established plasmonic materials. Biomolecule tests were performed to determine the ability of the device to respond to binding events at the surface that cause changes in the refractive index. The nanohole array acted as a transducer during these biomolecule recognition experiments and demonstrated the potential of designing a practical device integrating this transduction method. Theoretical simulations of the nanohole array were performed using Lumerical software to confirm the results of this experimental characterization. Furthermore, an optimization of the pitch of the nanohole array was calculated theoretically to obtain maximum transmission for the highest sensitivity .

Preliminary studies on the integration of an MIP recognition layer were also performed. This biomimetic recognition element can be created for any molecule, is stable in a range of environments, is reusable, and can be easily applied on many surfaces. The replacement of biomolecule recognition elements with MIP will greatly decrease the cost and increase the stability of biosensors. The MIP is formed by crosslinking around a target molecule which is then removed. Thus the target molecule is the only molecule that can fit into the imprint, which is why the MIP has such high selectivity. A novel polymer was used for the MIP layer, which may present additional cost and stability advantages over existing materials.

Rhodamine 123, which is a green fluorescent dye easily detectable by fluorescent microscopy, served as the template molecule. The detection of target molecules of the MIP was demonstrated by the presence of Rhodamine 123 in the film after incubation in a solution. The sample was then washed to remove the recognized target molecule, thereby demonstrating the reusability of the MIP recognition layer. Transmission spectroscopy was performed to determine the effect of MIP recognition on the transmission spectrum, but the results were inconclusive. The best range of thicknesses for the MIP layer on the surface of the nanohole array transducer was determined through the examination of the effect of deposited non-imprinted polymer layers with varying thicknesses on the transmission spectrum.

1.3 Thesis Outline

This thesis is organized in such a way to enable understanding of the fundamental concepts of refractive index sensing, followed by discussion of fabrication and characterization methods, theoretical predictions, experimental results, and analysis. The thesis begins in Chapter 2 by discussing the background of the device and the operational principles of using a nanohole grating as a refractive index sensor. The basic functionality of a refractive index sensor and the fabrication methods are explained in this chapter.

Chapter 3 discusses the materials used during fabrication and experimentation as well as the methods used to characterize the nanohole array. The experimental procedures used to obtain relevant data from these methods are outlined and the importance of each characterization method is mentioned. Several external factors that can influence the characterization and operation of the device as a refractive index sensor are mentioned.

The theoretical origin of the transmission spectra for each grating is explored in Chapter 4. First, different originations of general transmission spectra are explained. The cause of each individual grating is discussed.

The results from the experimental tests are presented in Chapter 5. These results and their implications are further discussed in Chapter 6. The possibility of using the nanohole array as a transduction element in a biosensor is evaluated. Chapter 7 provides some concluding remarks and indicates the future direction of research for this project.

Chapter 2

Biosensing with Nanohole Arrays

2.1 Biosensor Classification

A biosensor consists of two main elements, a recognition element and transducer element, which work together to determine concentrations of analyte in a solution. Most biosensors are affinity based, meaning that they detect a change at the interface between the recognition and detection elements instead of detecting an analyte in a solution. There are detection methods which use labels to tag target molecules for identification, and label-free methods which directly detect the binding event between a target molecule and recognition element. These methods will be discussed in this section along with the two main components of a biosensor, beginning with the recognition element.

2.1.1 Recognition Element

Recognition elements are biological or biologically derived components that can specifically bind to analytes in a sample and produce a signal. Examples of recognition elements include receptors-such as, enzymes, antibodies, nucleic acids- molecular imprints, and lectins In affinity biosensors, the selectivity of the sensor is the ability of the sensor to respond only to the analyte and no other molecules. Molecular recognition occurs naturally through specific interactions between compatible molecules, such as antibodies binding with viruses. These natural binding pairs are exploited as recognition elements in biosensors by attaching one of the elements to the surface of a transducer, which can then selectively bind to their biological counterparts. However, traditional

biological recognition elements such as antibodies, enzymes and DNA, are unstable when not in their native environment. Also, these traditional biolgical recogntion elements are often in short supply and operate under restricted conditions.[9] Lastly, not all molecules have natural binding counterparts and therefore cannot be detected in this way.

For these reasons, biomimetic recognition elements, such as Molecularly Imprinted Polymers (MIPs) have been a growing research topic. A MIP is a polymer network imprinted with the shape of a specified template molecule that can selectively recognize that template molecule in a sample solution.[10] MIPs offer superior stability to biomolecules when exposed to solvents and extreme temperatures, are reusable, have a binding affinity comparable to traditional biological receptors, are cheaper to produce, and allow customized preparation to enable large scale chip production.[11] MIPs can be easily deposited on the surface of the transducer element by a number of methods including spin-coating, which is much faster and more cost effective than the immobilization of biomolecules on the surface of the transducer element.

2.1.2 Transduction Element

The transduction element in a biosensor converts the analyte-recognition element binding phenomenon to a measureable signal. There are many different kinds of transduction elements including optical, piezoelectric, electrochemical, etc. In particular, optical transducers exhibit important features such as fast analysis time, thereby enabling real time detection, high sensitivity, and use in non-purified samples.[12] Optical transducers cause interference in electromagnetic radiation, which is detected by measuring the intensity or phase change in the radiation source. Typically, this light is in the visible range and the intensity of transmitted, absorbed, or reflected light is plotted against wavelength. The nanohole arrays used in this thesis use surface plasmon resonance (SPR) based optical transduction by aluminum to monitor binding events at the metal-dielectric surface. This type of sensing does not require the use of a label, which will be discussed in the next section.

2.1.3 Label-Based vs. Label-Free Detection

Label-based methods, often referred to as indirect detection methods, use two molecules for detection, the target and a labeled secondary molecule raised against the primary molecule host species.[13] The four main label-based detec-

tion methods are chromogenic detection, where the binding of the secondary molecule to the detected analyte produces a color, fluorescence-based detection, where the labeling molecule is fluorescent and therefore detectable by fluorescent imaging, radioactive labeling, where the labeling molecule is a radioactive isotope and chemiluminescence, where the binding of the secondary molecule to the detected analyte produces a chemical reaction that makes those molecules luminescent.[14] These methods have a high level of sensitivity and generate an intense signal that is easily measured. However, labeling a biomolecule can drastically change its binding properties,[15] affect the reaction kinetics of the sensor and increase the analysis time,[16] thereby increasing the cost and deceasing the efficiency of the device.

Label-free methods eliminate the need for traditional labels like fluorescent dyes or radioactive isotopes in biosensors. When an analyte binds to a surface sensitized by recognition elements, the resulting changes in that surface (i.e RI, resistance, etc.) are due solely to the presence of the target molecule as opposed to a secondary labeling molecule. Although these methods are not always as sensitive or selective as label-based methods, they decrease the cost of sensing, cut down on analysis time and allow for real-time detection of analytes.[17] This real-time detection of analytes can improve measurement accuracy and enables determination of affinity constants.[18] However, analyte binding to the surface produces a relatively small change in surface properties that occurs upon binding, therefore highly sensitive transduction methods are required to amplify the signal caused by these binding events.

2.2 Refractive Index(RI) Sensing

Nanohole arrays can detect refractive index(RI) changes in a solution to determine the concentration of analyte in a solution. The RI, n, quantifies how light propagates through a medium. Light traveling through air in a vacuum has a RI of 1, which is the reference value that all other refractive indices are based on. When a wavefront propagating in one medium comes into contact with another medium of higher RI, the wavefront "bends" due to the change in speed, as is shown in Figure 2.1. The velocity of radiation and wavelength change as the light propagates through different media.[19] Hence, index of refraction is a representation of how much the speed of a light beam changes as it moves from one medium to another.

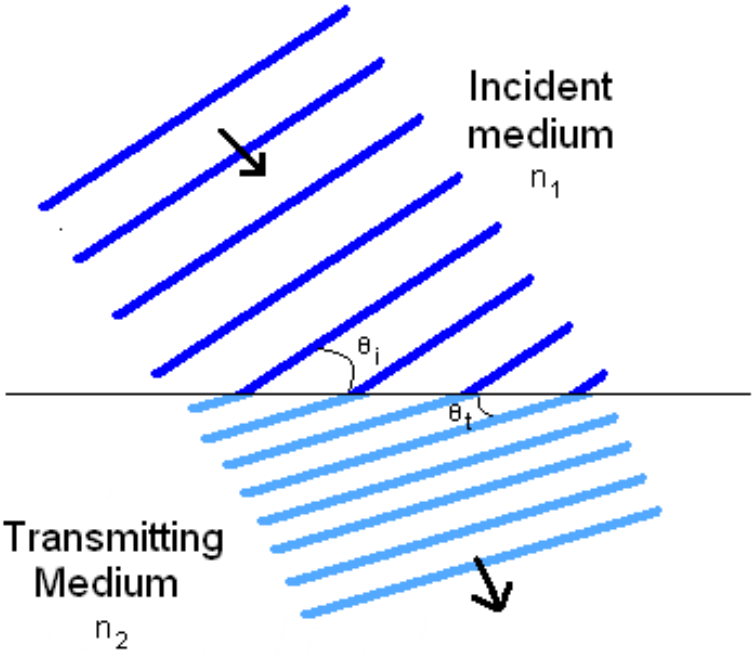

Figure 2.1: Refraction of waves at the boundary between two media of different RI.

Unlike refraction where light bends due to a change in velocity of the wave as it moves through different media, diffraction occurs when a wave encounters an obstacle and any part of the wavefront is altered in phase or amplitude. Classical physics describes diffraction as the apparent bending of waves around small obstacles and the spreading out of waves past small openings.[20] According to the Huygens-Fresnel principle, each point in the optical field can be considered as a point source, and the amplitude of the optical field at any point beyond the array of small openings is the superposition of all the point source contributions.[19] Therefore, because the wavelengths of light in the visible spectrum(400nm to 700nm) are large compared to the diameter of the nanoholes, the waves of light will spread out isotropically in large angles beyond the obstruction when the wavelength comes in contact with the nanohole grating at normal incidence, as depicted in Figure 2.2.

Beyond the nanohole array, these nearly circular waves interfere either constructively when they are in-phase or destructively when they are out-of-phase with each other. These additive and destructive components translate to peaks and valleys in the intensity of diffracted light vs. wavelength graph, which is also known as a transmission spectrum. Classical physics would predict that the transmission would be very weak through the nanohole array and thus difficult to detect due to the size of the holes and opaqueness of the metallic thin

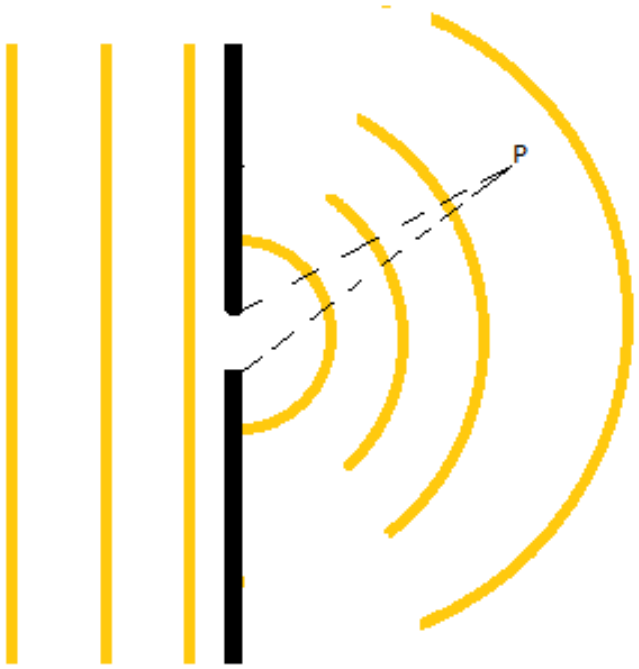

Figure 2.2: Diffraction of waves at a small aperature.

film. However, a unique phenomenon, called extraordinary optical transmission, occurs through the nanohole array that allows its tranmission spectrum to be measureable even in the far field regime.

2.2.1 Extraordinary Optical Transmission(EOT)

In 1998, Ebbesen et.al discovered that noble metallic films with regularly repeating sub-wavelength structures can couple light with oscillating valence electrons at the interface between the metal surface and a dielectric called Surface Plasmons(SPs), and gives rise to extraordinary optical transmission(EOT).[21] EOT is a unique phenomenon where transmission through a periodic grating structure is much higher than expected and is therefore easier to measure. When the incoming beam of light matches the momentum of a surface plasmon, it starts to resonate. Collective resonating SPs can sustain the propagation of electromagnetic waves on the surface of the metallic film, known as surface plasmon polaritons (SPPs). The coupling of the incident light with these SPPs gives rise to waves with larger amplitudes that can in-

terfere constructively or destructively to give enhanced transmission peaks and dips that can be measured even in the far field regime.[22]

2.2.2 Transmission Spectroscopy

Transmission spectroscopy studies the dispersion of electromagnetic radiation by matter through the measurement of intensity of transmitted light as a function of wavelength. This principle was used to detect changes in RI at the interface between the metallic surface of the nanohole array samples and dielectric medium. Because the RI of the surrounding medium has an effect on the momentum of light hitting the surface, it will change which SPs are resonating and therefore which SPPs will propagate along the boundary between the metallic surface and dielectric medium. Furthermore, the SPP that propagates along the metal-dielectric interface extends into each medium, so the characteristics of this wave depend on the material conditions near the interface. Hence, changes in RI along the interface have large effects on the transmission spectrum. The binding of analytes to the recognition element placed on top of the nanohole array changes the RI and therefore produces a shift in the transmission peaks.

2.3 Factors Effecting RI Sensing

There are several factors that effect light transmission through a nanohole array, including Rayleigh anomalies, Surface Plasmon Polariton-Bloch Waves, and Rayleigh Anomaly-Surface Plasmon Polaritons. These spectral features can exist on the top or bottom of the grating where it is touching a dielectric medium. The coupling of two of these features will lead to a large constructive or destructive interference, which will give rise to the peaks and dips in the transmission spectrum. Any change in the RI at the surface of the grating caused by a change in the dielectric medium adjacent to the metallic grating will directly effect these spectral features. Therefore it is possible to predict the position of peaks and dips in a spectrum once the spectral feature responsible for each tranmission peak or dip is identified.

2.3.1 Rayleigh Anomalies(RAs)

Rayleigh anomalies(RAs) are non resonant spectral features associated with the gratings that arise from the abrupt redistribution of energy when light is

diffracted at an angle parallel to the surface. They are sometimes called threshold anomalies because they occur at the point where a diffracted order changes from propagating at a angle less than 90°to an evanescent wave propagating at an angle greater than 90°, or vice versa.[23] Figure 2.3 is a schematic representation of the nanohole array under study, where region I corresponds to the substrate material, region II is the grating, and region III is the region above the grating.

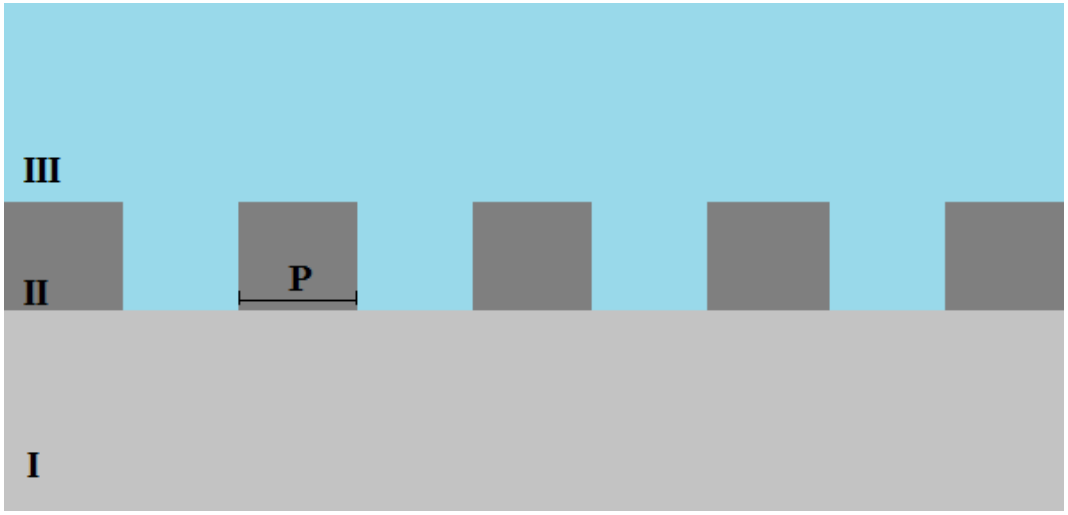

Figure 2.3: Schematic representation of the nanohole array system studied in this thesis.

The wavelength position of an RA can be predicted by equation 2.1,

$$\lambda_{RA} = \frac{P}{(w_1^2 + w_2^2)^{1/2}} n_X \tag{2.1}$$

where P is the pitch, (w_1, and w_2) are integer pairs corresponding to the particular order of the RA, $n_x = \epsilon_x^{1/2}$, and ϵ_x is the real, relative dielectric constant of medium X=I or III.[7] Medium I corresponds to the substrate that the aluminum gratings were deposited upon, therefore n_I was kept constant at the RI of the glass substrate(n=1.5). However, the RI on top of the grating could be varied by introducing different dielectric materials. Thus any peaks or dips in the transmission spectral arising from RAs would exhibit a wavelength shift in response to this variance of RI at the top metal-dielectric interface.

2.3.2 Surface Plasmon Polariton-Bloch Waves(SPP-BW)

According to Bloch's theorem, the energy eigenfunction of the wavefunction of a particle placed in a lattice with periodic potential can be written as the product of a periodic(Bloch) function with the same periodicity as the potential

and a plane wave envelope.[24] This wavefunction is a Bloch wave and can couple with an SPP of the same resonance to create a surface plasmon polarition-bloch wave(SPP-BW).

Because the metal nanoholes in Figure 2.3 are sandwiched between two different dielectrics, SPP-BWs excited at the interface between region III and II can tunnel through the nanoholes to the interface between region I and II, where they are scattered back into plane waves that contribute to transmission.[25] An n approximation for the free-space incident wavelength that can excite an SPP-BW is

$$\lambda_{SPP} = \frac{P}{(s_1^2 + s_2^2)^{1/2}} Re\left(\frac{\varepsilon_{Al}(\lambda_{SPP})\varepsilon_X)}{\varepsilon_{Al}(\lambda_{SPP}) + \varepsilon_X}\right)^{1/2} \tag{2.2}$$

Where (s_1, and s_2) are integer pairs corresponding to the particular order of the SPP-BW, P is the pitch,$\epsilon_{Al}(\lambda_{SPP})$ is the wavelength dependent relative permittivity of aluminum, n_x=$\epsilon_x^{1/2}$, and ϵ_x is the real, relative dielectric constant of medium X=I or III.[7] This equation can be used predict the position of SPP-BW waves through a nanohole array.

2.3.3 Rayleigh Anomaly-Surface Plasmon Polaritons(RA-SPPs)

The Rayleigh Anomaly-Surface Plasmon Polaritons(RA-SPP) effect occurs when an SPP-BW from one side of the metallic thin film is coupled with a RA on the other side, leading to a large increase in intensity of a narrow transmission peak over a small RI range. A simple relation can be obtained by equating the first order SPP-BW condition, (s_1, and s_2)=(1,0), on the region I substrate(n_I) with the first order RA condition,(w_1, and w_2)=(1,0), on the region III substrate(n_3), which is given in equation 2.3.

$$n_{III} = Re\left(\frac{\varepsilon_{Al}(\lambda_{RA-SPP})\varepsilon_I}{\varepsilon_{Al}(\lambda_{RA-SPP}) + \varepsilon_I}\right)^{1/2} \tag{2.3}$$

where λ_{RA-SPP} is the wavelength where the zero order SPP-BW and RA conditions are the same. This equation demonstrates the dependence of the RA-SPP wavelength on the RI. Any peak or dip originating from an RA-SPP in the transmission spectrum of a grating will therefore be affected by a RI change at the metal-dielectric interface. The relation between the periodicity of the grating and λ_{RA-SPP} simplifies to equation 2.4, which means the bulk sensitivity of a peak originating from an RA-SPP($dn/d\lambda$) simply becomes the periodicity of the grating.[7]

$$\lambda_{RA-SPP} = P \times n_{III} \tag{2.4}$$

2.4 Chapter Summary

In this chapter the principles supporting the use of RI sensing by nanohole arrays as a transduction technique were introduced, beginning with the basic principles of biosensing. The methods of classifying biosensors was discussed, recognition and transduction elements were introduced, and label-based and label-free methods of detection were compared. After an exploration of basic RI sensing principles, including RI and diffraction, the specific phenomena responsible for the ability of the nanohole array to act as a RI sensor were discussed. The spectral features responsible for transmission peaks and dips were then introduced. The next chapter provides insight into the materials and methods used to fabricate and characterize the nanohole arrays as RI sensors and introduces the characterization equipment used during experimentation.

Chapter 3

Materials and Methods of Characterization

3.1 Nanohole gratings fabricated on metallic substrates

The last chapter provided the theoretical basis for a nanohole array transduction device, but it is necessary to quantify these claim by characterizing the device. Nanohole gratings with 1 μm and 500 nm pitches imprinted on metallic substrates were characterized as potential transducer components of RI sensors by several methods including bulk sensitivity and thickness sensitivity. The materials involved in the fabrication of the nanohole arrays and characterization experiments are introduced in this chapter, and the procedures used to characterize the device are described. Traditional and synthetic recognition elements were attached to the surface to evaluate the operation of the integrated RI sensing device. The effect of light polarizatioon was also examined. The characterization equipment used during all experiments is mentioned and the operation of th device is elucidated.

3.1.1 Fabrication of gratings

The nanohole grating structures analyzed during this project were fabricated at the Instituto de Sistemas Optoelectrnicos y Microtecnologa, Universidad Politcnica de Madrid (ISOM-UPM). First, an aluminum layer was deposited onto a previously washed 200 μm glass substrate by technicians at UPM ISOM using a Varian VT 118 Electron Beam Physical Vapor Deposition (EBPVD) machine. This process occurs under high vacuum where an electron beam generated by a charged tungsten filament bombards an alumina anode

causing atoms of aluminum to transform into the gaseous phase. When evaporated, alumina dissociates into aluminum, AlO_3, and Al_2O. The aluminum atoms then precipitate into solid form and form an even coating on top of the glass substrate.[26] The deposition rate was carefully controlled, leading to a fairly even film thickness of 100-130nm. Aluminum was used as the grating material due to its low cost, compatibility with available fabrication and characterization machinery, and ready availability.

A nanohole grating pattern is determined based on the desired pitch of the RI device. The separation of the nanoholes is comparable to the desired pitch of the grating. A nanohole grating pattern template was formed on top of the aluminum layer using a nanolithography process. A ZEP520 positive resist layer was spin coated on top of the aluminum layer using a Coater CONVAC 1001 spin coating system at 5000rpm for two minutes. The sample was then baked for two minutes at 190°C to remove the solvent, improve resist adhesion to the substrate, and prevent bubbling during etching.

The nanoholes were then imprinted into the resist using a CRESTEC CABL-9500C high resolution electron beam nanolithography system. The machine was programmed to print the holes in a square grating pattern of specified pitch that was repeated multiple times to get the proper length and height of the desired grating. After the nanolithography process was complete, the resist was developed by a ZED-N50 commercial developer for the employed resist. Finally, the nanohole grating pattern was transferred to the aluminum through an inductively coupled plasma(ICP)chemical etching process. The remaining resist was removed by soaking the nanohole array system in a 60°C 1-methyl-2-pyrrolidone bath for ten minutes, and thoroughly washing the device in deionized water.

The resulting gratings were viewed under a scanning electron microscope (SEM) to determine the extent of the etching process and the size and shape of the holes. The SEM image of the 1μm grating, shown in Figure 3.1, has a pitch of 0.970μ, which is very close to the intended pitch. It is important to note that the size and shape of the holes are not identical to one another in these gratings, which has an effect on the transmission spectrum. The 500nm grating, shown in the SEM image of Figure 3.2, has a pitch of 496nm, which is the closest achieved to that intended. It is easy to see the variation in the size and shape of the holes in this image due to the close spacing of the holes.

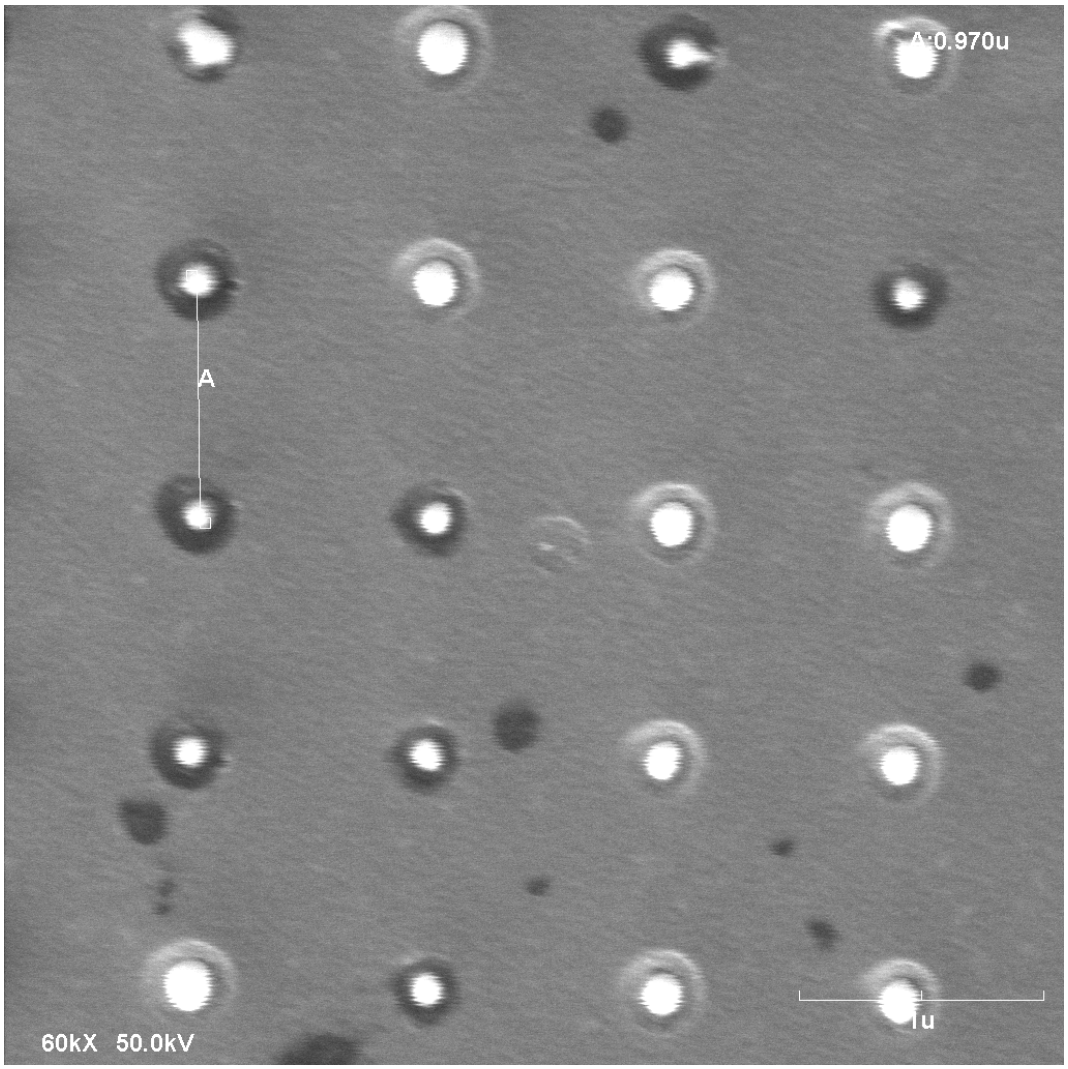

Figure 3.1: SEM image of 1μm grating displaying the pitch.

3.1.2 Nanohole Grating Solvent Characterization

The gratings were physically characterized by analyzing the changes in their transmission spectra with varying factors. A Jasco V-650 spectrometer was used to measure the transmission spectral response in all the experiments, and a quartz cuvette was used as a sample holder for the gratings. The transmission spectra analyzed were in the visible light regime within the wavelength range 400nm to 900 nm. The optimal peak for sensing applications of each grating was determined from the spectral response of the grating when exposed to liquids of varying RI. As the RI increased, a red shift of the spectra was noticed in all of the gratings. The optimal peak for sensor response is the peak that shows the greatest red wavelength shift with increasing RI. The liquids

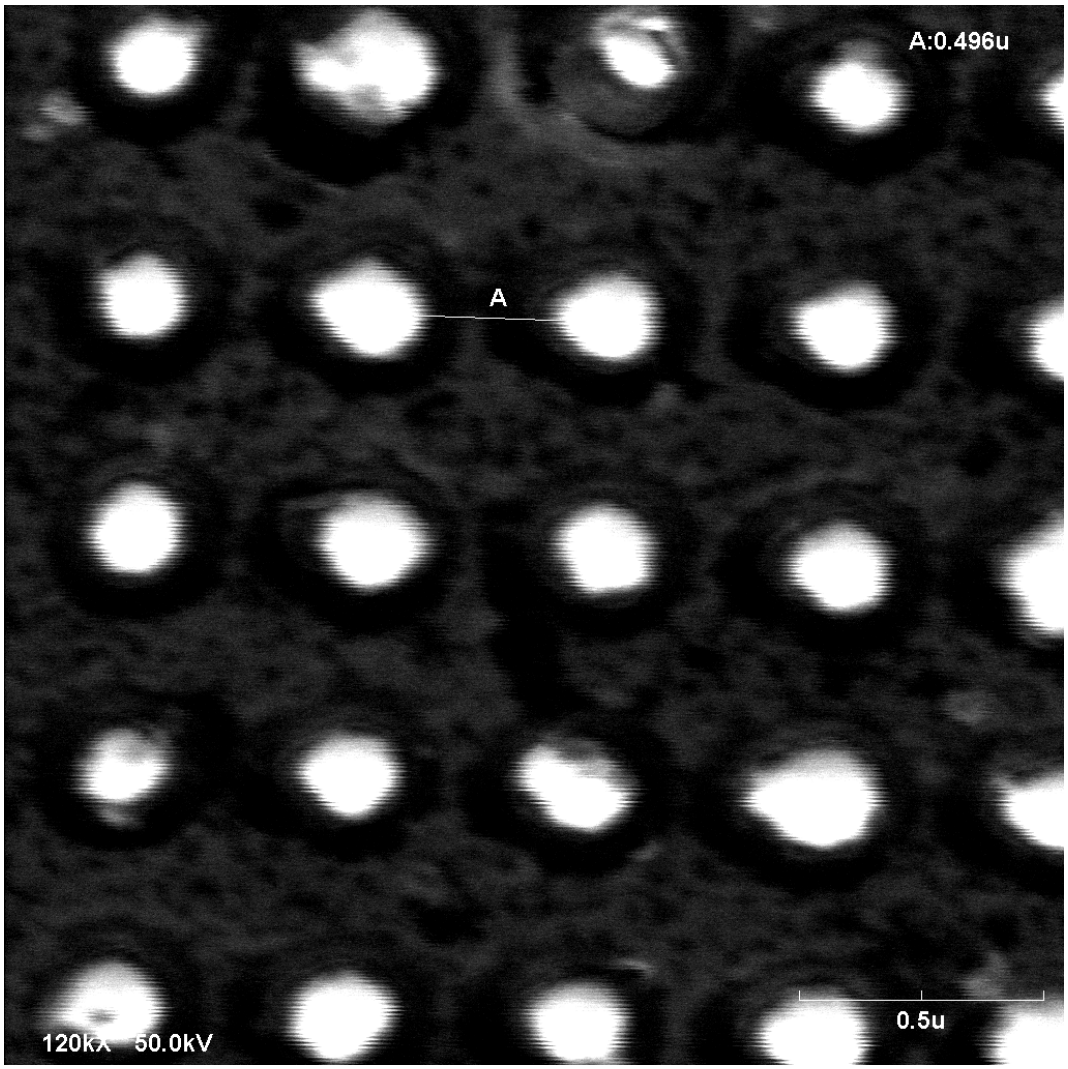

Figure 3.2: SEM image of 500nm grating displaying the pitch.

used during the experiments were methanol, ethanol, isopropanol(IPA), cyclohexane, tetrahydrofuran(THF) and toluene. The refractive indices of these liquids are given in Table 3.1. Matlab was used to process the transmission data and determine the position of the peaks in the spectrum.

The bulk sensitivity, S_λ, is determined by the spectral change of the grating in response to varying RI ($dn/d\lambda$).[27] The higher the spectrum shift with changing RI, the more sensitive the device will be. The same liquids, shown in Table 3.1 as those used to determine the optimal peak for sensing applications were used in the bulk sensitivity experiments. The measurements were performed at room temperature(23°C±4°C).

Table 3.1: Refractive Indices of Liquids used During Experimentation

Methanol	Ethanol	IPA	THF	Cyclohexane	Toluene
1.362	1.361	1.367	1.407	1.425	1.496

The optimal peak wavelength position was then plotted against the varying RI in Microsoft Excel. A linear regression model was used to determine the relationship between the RI and wavelength shift. The slope of the linear regression gives the bulk sensitivity of the grating, which is expressed in nanometers per refractive index unit(RIU). The coefficient of determination, R^2, was also obtained from the linear regression model. It is a unit less quantity used to evaluate how closely the model fits the data. For any given linear regression line, an R^2 value exceeding .8 was considered an acceptable fit for the data and any value exceed .98 is considered a very close match.

3.1.3 Deposited Film Thickness Sensitivity

Polymer layers of varying thickness were deposited on top of the nanohole grating RI device to determine the sensitivity of the grating to deposited layer thickness, which is important in optimizing the interaction between the transducer and recognition elements of the device. Poly(methyl-methacrylate) (PMMA)was used as the deposited layer material. The thickness of the PMMA film was controlled using a combination of cholorobenzene addition to decrease viscosity and varying spin-coating speeds. After the PMMA was mixed with the proper amount of chlorobenzene and a thin layer of polymer was achieved on the aluminum surface of the sample, the polymer was polymerized by baking the sample for 2 minutes at 160°C. Film thicknesses and refractive indices of the films were determined by the UPM ISOM Filmetrics F20 system. The thicknesses of the films measured were 105.4nm, 80.1nm, 42.9nm, and 28nm. Deposited layer experiments were performed on 1μm and 500nm pitch grating samples for insight into the effect of deposited layer thickness on gratings of various pitch.

3.1.4 Polarization Effect

Electromagnetic waves consist of several wave components that oscillate in different directions, called the polarizations of the wave. These polarizations can be isolated by polarizers like the schematic diagram of polarization in

Figure 3.3. It is possible to optimize the coupling strength between incident light and SPPs by adjusting the incident light polarization.[28] The effect of polarization on the transmission through the nanohole array was examined by adding a polarizer in front of the light beam before it hit the sample and blocking various polarizations of light, including, 0°, 45°, 90°, and 180°.

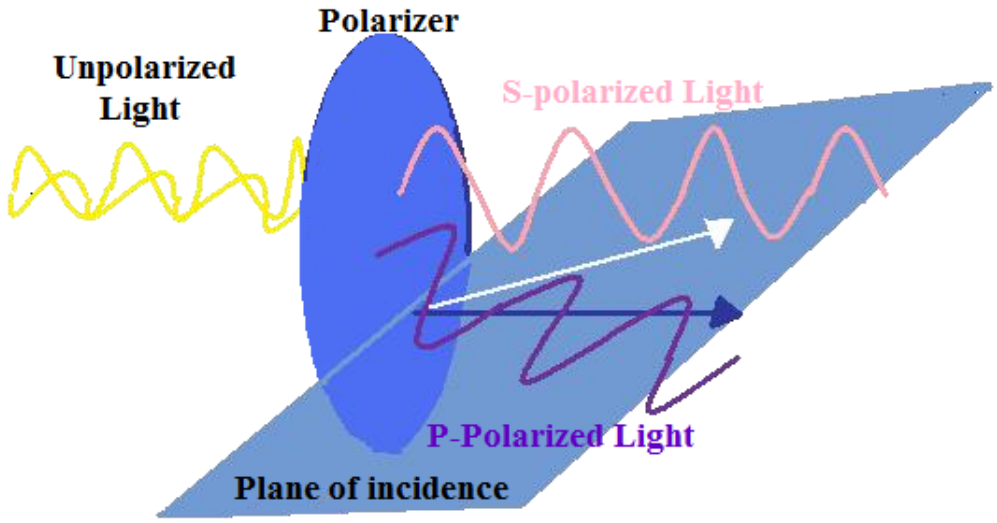

Figure 3.3: Demonstration of polarized light

3.2 Biomolecule Recognition Element

Biomolecule recognition elements in biosensors are natural receptors such as antibodies, enzymes or cyclic sugars.[29] The surface of the transducer element in the biosensor is functionalized by these molecules to detect analytes in a solution. Biomolecules are immobilized on the surface of the transducer and then perform their normal functions. For example, an antibody will bind to a viral strand. This natural selectivity identifies the presence or concentration of an analyte that the transducer can then translate into a readable output. In order to attach the biomolecule to the surface, the surface must first be functionalized.

3.2.1 Surface Functionalization

The functionalization of the surface of the nanohole grating patterned aluminum samples determines the ability of the sample to interact with its environment and selectively immobilize specific analytes on the transducer surface.[30] In this case, microcystin-leucine-arginine (MCLR), a very common and potent cyanotoxin found in water that is capable of producing a number of harmful side effects in humans and animals, was used for the biomolecular recognition experiments. First, the aluminum surface of the sample must be modified with organofunctional silanes to provide suitable attachment sites on the surface for covalent bonding of the MCLR to occur. An aminopropyltriethoxysilane, which has a terminal amine group, was used as the silane because of the availability of an amine reactive group on the MCLR. Following the procedure of the liquid phase method of silization, the sample was cleaned thoroughly and then immersed in a silane solution. Once the surface was silanized, the MCLR was covalently bonded to available amide groups on the surface. The MCLR was immobilized on the surface and ready to selectively detect MCLR antibodies in water samples. The complete procedure used to functionalize the biomolecule on the aluminum surface of the sample is the same as that outlined by S. Herranz et.al. The functionalization of the nanohole grating imprinted metallic films was performed by S. Herranz at the Universidad Complutense de Madrid.[31]

3.2.2 Detection Protocol

The general procedure for biomolecule recognition involves exposing the samples with immobilized MCLR on the surface to water samples containing MCLR antibodies. The immobilized MCLR biomolecules on the surface will bind to the MCLR antibodies contained in the water samples which should register an effect in the transmission spectra of those samples. The exposure of the samples containing immobilized MCLR on the surface was performed using the protocol outlined S. Herranz et. al.[31] Transmission spectra measurements were taken by a spectrophotometer.

3.3 Molecularly Imprinted Polymer(MIP) Recognition Element

MIP is created by a templating process at the molecular level. During this process, the polymer is developed around a molecule, which is then extracted, leaving corresponding imprints behind. The MIP is then able to bind targeted molecules in a solution with similar shape and specificity, making MIPs highly selective.[11] This process can be applied to many different organic and inorganic molecules, which makes MIP technology extremely versatile and widely applicable, especially as the recognition element in biosensors. Synthetic recognition elements like MIP remove many of the limitations that biomolecule recognition elements impose on biosensing technologies, making the technology cheaper and more applicable in a variety of situations. MIP in particular has selectivity comparable to traditional biomolecules with the added advantages of being capable of producing receptors for a variety of molecular structures, enabling large-scale chip fabrication, and offering superior stability when exposed to solvents and temperature extremes.[32]

3.3.1 Fabrication

During the MIP formation process, functional monomers are assembled around a specified target molecule and then fixed by crosslinking around the target molecule during polymerization. The functional monomers are held together by either noncovalent (Figure 3.4(a)) or covalent forces (Figure 3.4(b)), including electrostatic, hydrogen bonding and hydrophobic interactions. Covalent imprinting produces a higher yield of imprinting sites and is more efficient, but noncovalent imprinting allows a wider range of monomers, target molecules, and imprinted materials.[33] After polymerization has finished, the template is removed by extraction with solvents/ hydrolysis for noncovalent imprinting, or by chemical cleaving from the polymer for covalent imprinting, which leaves behind sites similar in size and shape to the template molecule.

A methacrylate based novel polymer was used to make the MIP layer during experimentation. This polymer was mixed with 30μg/mL of 6-amino-9-(2-methoxycarbonylphenyl)[xanthen-3-ylidene]azanium chloride (Rhodamine 123), which was the template molecule that was used to demonstrate the MIP's selective binding ability during experiments. Rhodamine 123 was chosen due to its green fluorescence which is easily detectable by a fluorescent microscope.

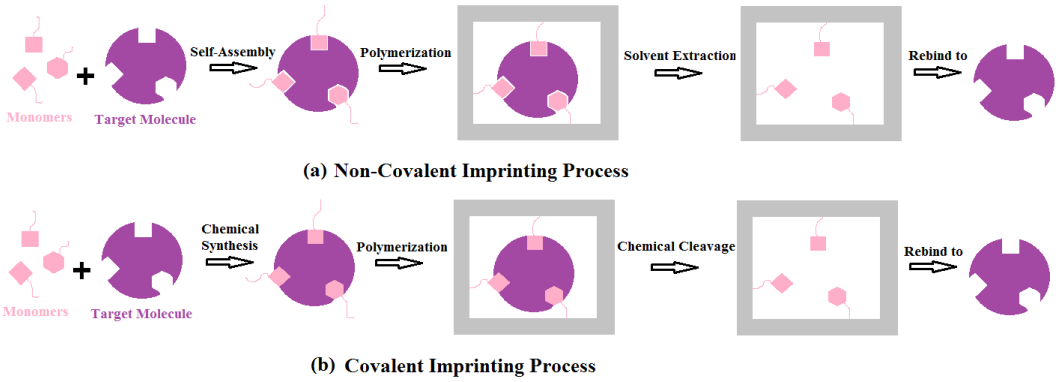

Figure 3.4: Schematic overview of the (a) noncovalent and (b) covalent molecular imprinting techniques

The polymer containing molecules of Rhodamine 123 was spin-coated on top of the aluminum layer of the sample imprinted with a nanohole grating. After an even layer of polymer mixture is distributed on the sample, a region of the polymer mixture was defined over the grating structure of the sample using a photolithography process. After exposure, the sample was developed with THF to remove any unwanted polymer mixture from the regions surrounding the grating structure. The remaining polymer mixture was crosslinked around the Rhodamine 123 molecules through heating at 175°Cfor one hour. At the same time, a reference sample of non-imprinted polymer(NIP) was created in a similar fashion on a separate sample with the same nanohole grating pitch. However, the polymer did not contain Rhodamine 123 molecules so the final film was just a layer of the polymerized polymer. The now crosslinked polymer surrounding the Rhodamine 123 template molecules was washed in Methanol three times for one hour each time in order to remove the template molecules. This process leaves behind the molecular imprints in the polymer which can now be used as a recognition element. Fluorescent microscopy was used to ensure the complete removal of the Rhodamine 123 template molecules from the crosslinked polymer.

3.3.2 Detection Protocol

Before incubation, the transmission spectra of the MIP covered nanohole grating sample and the NIP reference sample were taken using a spectrophotometer. The nanohole grating imprinted metallic sample with MIP layer was then incubated in a solution of 4ml hydrogen cyanide(HCN) with 30μg/mL

of Rhodamine 123 for a total of 18 hours. The sample was then dipped in Methanol and dried with Nitrogen gas to prevent incubation solution build up at the surface from affecting the measurements. The transmission spectra and fluorescent images of both the MIP and NIP covered samples were taken to determine if there was any recognition by the MIP and how effective the nanohole grating imprinted metallic films were at detecting this recognition.

3.4 Characterization Equipment

The experimental methods discussed above use various equipment, including a spectrophotometer, a flourescent microscope, and a film analyzer for characterization of the nanohole array. This section explains the operation of this equipment and how it was used to evaluate the performance of the nanohole gratings as transduction elements. The spectrometer was used to measure changes in the transmission spectrum of the nanohole array in response to varying factors, such as different dielectric media on the top of the nanohole array. The flourescent microscope was used to confirm the presence of target analyte during the MIP recognition experiments, while the film analyzer determined the RI and thickness of deposited layers. The spectrophotometer, which measures light intensity as a function of wavelength, was the most frequently used piece of equipment.

3.4.1 Spectrophotometer

In its simplest form a spectrophotometer consists of a white light source and a detector placed on opposite sides of the sample being measured. As light passes through the sample it diffractsand the intensity of light within the detectors angular range is captured and translated by software into a readable output. This output is usually a graph of transmittance, absorption or reflectance vs. wavelength of light.

A Jasco V-650 spectrometer belonging to UPM ISOM was used to make the measurements of the transmission spectra through the nanohole grating patterned samples. This research tool uses a light source with a broad range of wavelengths from 400nm into the infrared range, although only wavelengths in the visible range from 400nm to 850nm were used to achieve the transmission spectra. The spectrophotometer uses slightly more complicated optics to focus the beam through the sample but generally works in the same way as

described above. However, because the sample used had a nanohole grating pattern on a semi-transparent aluminum film, much of the transmitted light was greatly dispersed and the detector could not collect all of the transmitted light. Therefore, an integrating sphere was used to focus all transmitted light into the detector. Then the Jasco V-650 software was used to process the information and produce a graph of transmittance(%) vs. wavelength(nm), such as the example spectrum of methanol shown in Figure 3.5.

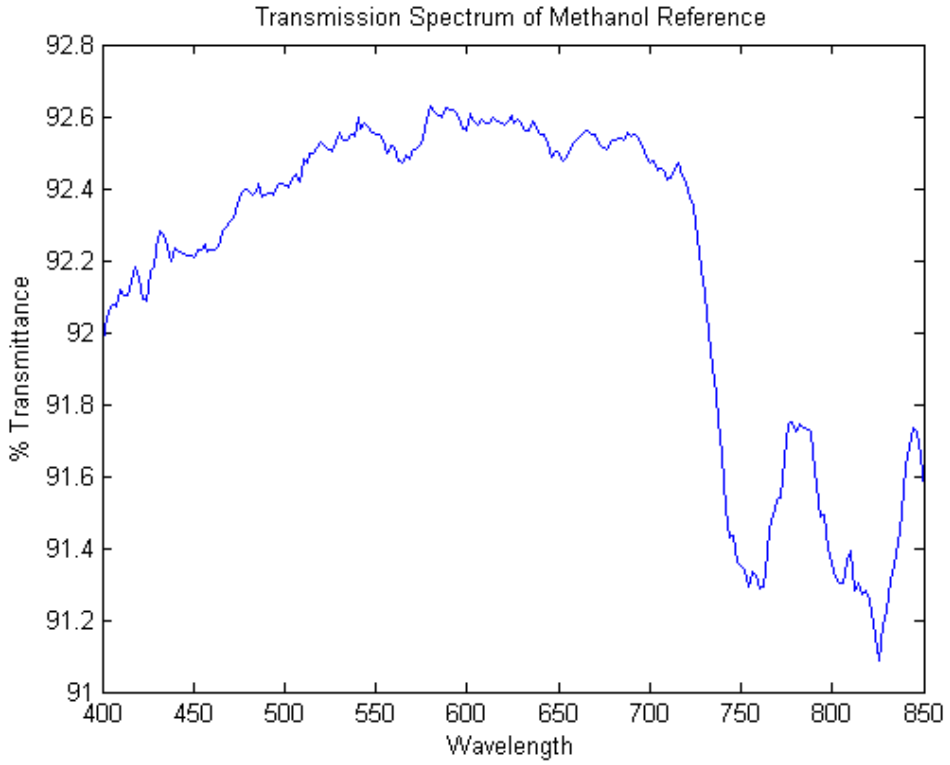

Figure 3.5: Example of a transmission spectrum, Methanol reference in quartz cuvette

3.4.2 Fluorescent Microscope

Fluorescent microscopes irradiate a material with a high intensity beam of light at a specific wavelength. Certain materials will then emit energy of a much longer wavelength in the visible regime which is viewed as a magnified image of the original sample. An Olimpus X51 confocal fluorescence microscope with a 488 nm interferential filter and 600nm dichroic mirror was used to perform flourescent microscopy of the samples. There was a cut-off in emission between camera and dichroic at 570 nm to avoid interferencial external light. This technique was used to detect the presence of Rhodamine 123 dur-

ing the MIP recognition experiments because it appears fluorescent under the microscope while the other materials in the sample do not.

3.4.3 Filmetrics

A Filmetrics F20 thin film analyzer was used to simultaneously determine the thickness and RI of thin film layers on the nanohole grating patterned samples. The analyzer measures light reflected through the sample and analyzes this light over a range of wavelengths. Because of the wave-like nature of light, oscillations arise from the addition of waves reflected off the top and bottom interfaces of the thin film that are either in-phase(waves add constructively) or out-of-phase(waves add destructively) depending on the wavelength of light, and thickness and optical properties of the film. These intensity oscillations are expressed in a reflectance spectrum, similar to that in Figure 3.6. The period and amplitude of these oscillations can be used to determine thickness and RI of the thin film. The Filmetrics F20 measures intensity oscillations

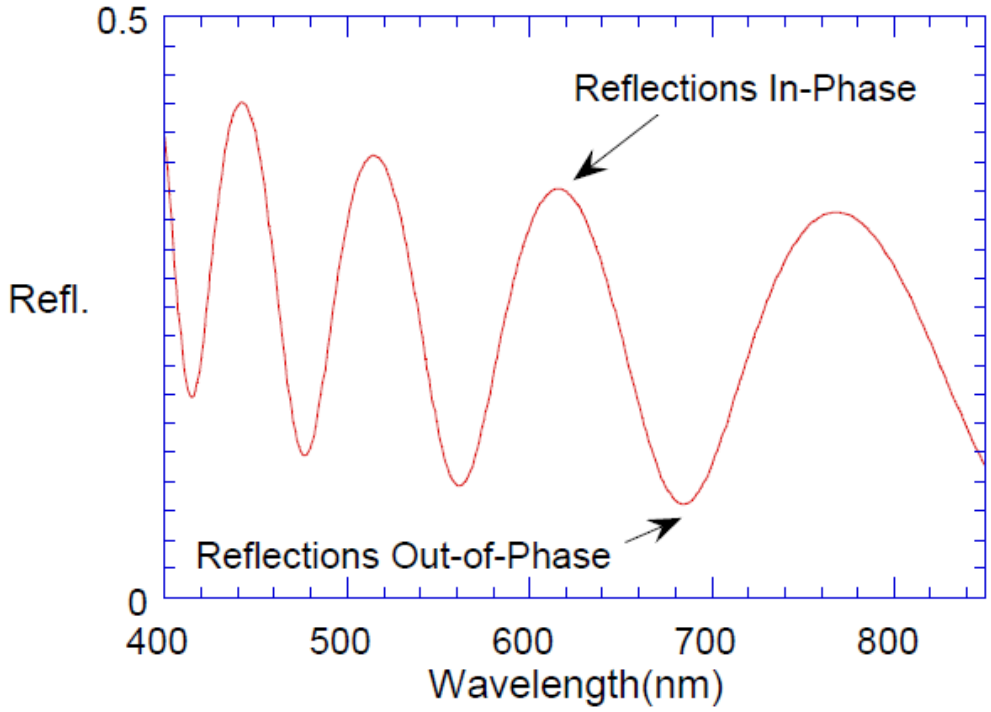

Figure 3.6: Example of a reflectance spectrum with oscillations for the Filmetrics F20[34]

from reflecting light through a thin film sample and calculates a reflectance spectrum correlating to the measured spectrum. It performs a simultaneous

analysis of thickness and RI of the thin films by varying RI to optimize the correlation between the calculated and measured reflectance spectra.

3.5 Chapter Summary

The materials used in the fabrication and characterization of the nanohole array RI sensor were discussed in this section. The fabrication methods of the nanohole array, biomolecule recognition element, and MIP recognition layer were explained, as well as the methods of detection used to determine the ability of the nanohole array to act as a RI sensor. The basic operating principles of the equipment used for characterization of the device was also discussed. In the next chapter, the origins of the transmission spectra of the nanohole gratings will be explored as well as the theoretical characterization and optimization of the nanohole array as a RI sensor.

Chapter 4

Theoretical

In order to optimize the design of the nanohole grating RI sensing device for biomolecule recognition, finite-difference time-domain(FDTD) simulations were performed. Lumerical FDTD solutions were used to optimize the pitch and thickness of nanohole grating patterned aluminum films. This software uses the finite-difference time-domain(FDTD) method to solve Maxwell's equations in 3D and is capable of analyzing the interaction of UV, visible, and IR radiation with the sub-wavelength periodic structures imprinted in aluminum films. The origins of the transmission spectra, including RAs, SPP-BWs, and RA-SPPs, of the gratings characterized in this thesis are discussed here. The nanohole grating has great potential to couple light into a waveguide, which is also discussed.

4.1 Finite-Difference Time-Domain(FDTD) Simulations

The finite-difference time-domain(FDTD) method is a numerical analysis technique that solves Maxwell's equations for electric and magnetic field distributions in the time-domain. This technique enables it to simulate many frequencies at one time in a discretized spatial domain in order to model the interaction of the electromagnetic field with physical objects. The central difference approximation is used to discretize the time-dependent Maxwell's equations in both the spatial and time domains.

The Maxwell-Faraday and Maxwell-Ampere laws are given by Equations 4.1 and 4.2, respectively,

$$\bigtriangledown \times \vec{E} = -\mu\partial\frac{\vec{H}}{\partial t} - \sigma_M \vec{H} \tag{4.1}$$

$$\bigtriangledown \times \vec{H} = \varepsilon \frac{\partial \vec{E}}{\partial t} - \sigma \vec{E} \tag{4.2}$$

where $\vec{E}$ is the electric field, $\vec{H}$ is the magnetic field, μ is the magnetic permeability, ϵ is the dielectric permittivity, and σ is the electric conductivity. These equations can also be expressed in the form of six directionally dependent field equations in Cartesian coordinates that describe anisotropic materials by using different values of dielectric parameters along the different directions.

The FDTD solution is reached by numerically solving the finite-difference equations resulting from discretizing Maxwell's equations in a leapfrog manner, meaning that the electric and magnetic field vector components in a volume of space are solved one after another at consecutive instants in time.[35] This solution is second order accurate and stable if the time step satisfies the Courant condition:

$$\Delta t \leq \frac{1}{c\sqrt{\frac{1}{\Delta x^2} + \frac{1}{\Delta y^2} + \frac{1}{\Delta z^2}}} \tag{4.3}$$

where c is the speed of light, and Δx, Δy, Δz are the time steps of the discretizations in the x-, y-, and z- directions, respectively.

The computational domain of the simulation is typically discretized using a rectangular unit cell with the electric and magnetic vector field components spatially staggered around the cube as proposed in Yee's scheme, shown in Figure 4.1.[36] This domain must be established in any FDTD calculations as it defines the region over which the simulations are performed and the electric and magnetic fields are determined at every point inside this space.

4.1.1 Lumerical Software

Numerical analysis of the nanohole grating geometry was performed with FDTD Solutions by Lumerical Solutions, Inc. This software is capable of analyzing the interaction of UV, visible, and IR radiation with the nanohole array structure,. However, only the spectrum from 400nm to 850nm was used during simulations. The software follows the same general procedure described above for determining the FDTD solution. The algorithm splits the discretized Maxwell's equations into two independent sets of equations composed of three vector quantities that can only be solved in the x-y plane. The TE (transverse electric) equations include the x and y components of the electric field and the z component of the magnetic field, where as the TM (transverse magnetic)

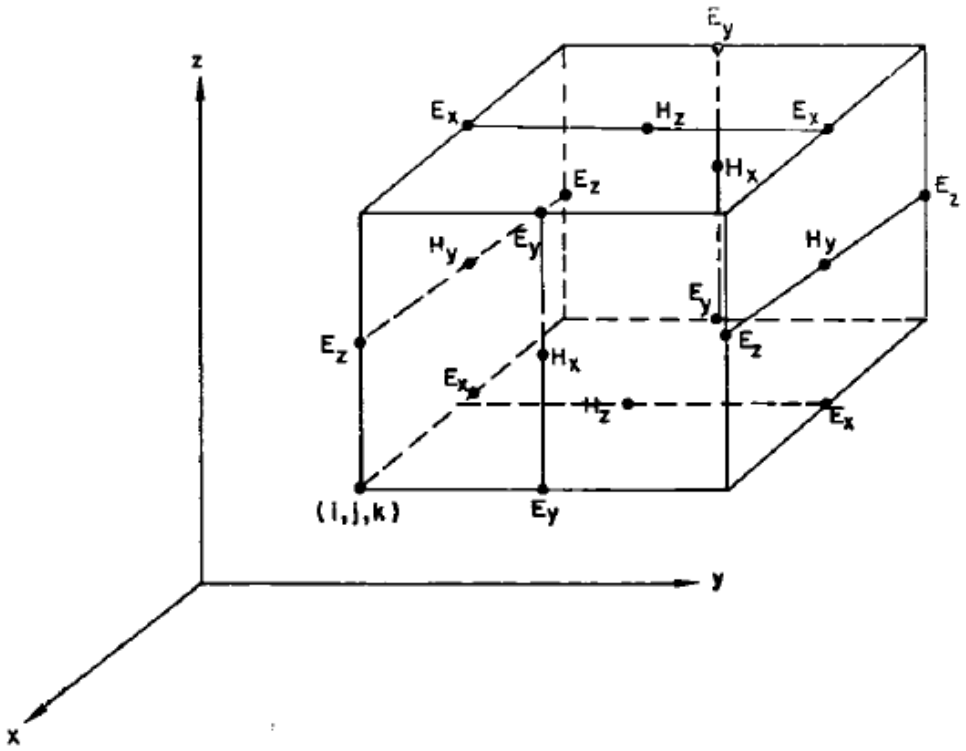

Figure 4.1: Position of the field components in Yee's cell. The electric field components are in the middle of the edges and the magnetic field components are in the center of the faces such that each electric(E) field vector component is located midway between a pair of magnetic(H) field vector components, and vice versa.[36]

equations include the z electric field component and the x and y magnetic field components.

The Lumerical software uses a rectangular Cartesian coordinate mesh as the computational domain. At each mesh point, the electric and magnetic fields are calculated. Using a smaller mesh gives a more accurate representation of the device, but also increases the simulation time and memory requirements.[37] Because the grating was periodic, the FDTD region was composed of a single unit cell shown in Figure 4.2. The radius and the thickness of the aluminum layer were kept constant at 150 nm and 80 nm, respectively, which were their average measured values during experimentation. The bottom dielectric, which represents the glass substrate underneath the nanohole array fabricated in aluminum, had a constant RI of 1.5, but the top dielectric was varied during simulations. It was assumed during simulations that the nanoholes penetrated the aluminum completely and reached the glass, although in actuality there

would be a cone-like cavity instead of a perfectly cylindrical one due to errors during fabrication.

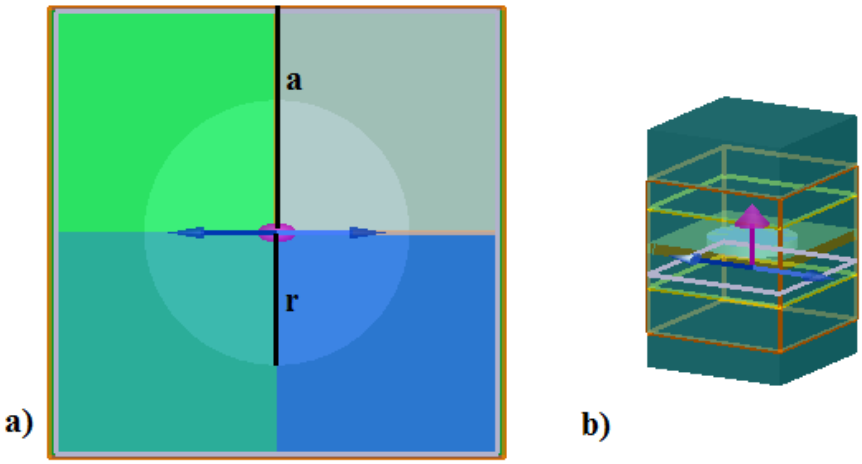

Figure 4.2: Images from the Lumerical saoftware of (a)the FDTD region simulated where a is the pitch of the grating and r is the radius of hole, (b) 3D view of the grating including upper dielectric region, nanohole array, and lower dielectric substrate

Simulations were performed to compare with the experimental results of the effect of varying solvents on nanohole arrays with 500nm and 1μm pitches. All conditions of the nanohole array structure were kept constant except for the RI of a simulated dielectric layer on top of the nanohole. Additionally, the effect of deposited thick layer(200nm-1.5μm) and thin layer(30nm-100nm) thicknesses on the transmission spectrum of the nanohole arrays was performed on the two different pitched gratings. Again the RI of the simulated top layer dielectric material was varied, but the RI did not vary as greatly with thickness as with solvents. Thus, smaller RI changes of the dielectric were simulated. It was assumed that thick layers completely filled the nanoholes, while thin layers did not. Therefore, these were the conditions imposed in the simulations to differentiate between thick and thin layers.

An optimization study of the pitch was also performed to determine the optimal grating structure to use for the device. A maximum transmission parameter, which represented the maximum transmission of the highest peak, was created and the optimization swept across various pitches to maximize this high transmission.

4.1.2 Simulation Results

Solvent characterization of the 500 nm and 1 μm pitch nanohole arrays were performed theoretically using Lumerical. The spectral comparison of the 500 nm grating is shown in Figure 4.3, while the linear relationship between RI change and wavelength red shift is demonstrated in Figure 4.4. The spectral comparison and linear relationship between RI change and wavelength shift of the 1 μm are shown in figures 4.5 and 4.6, respectively.

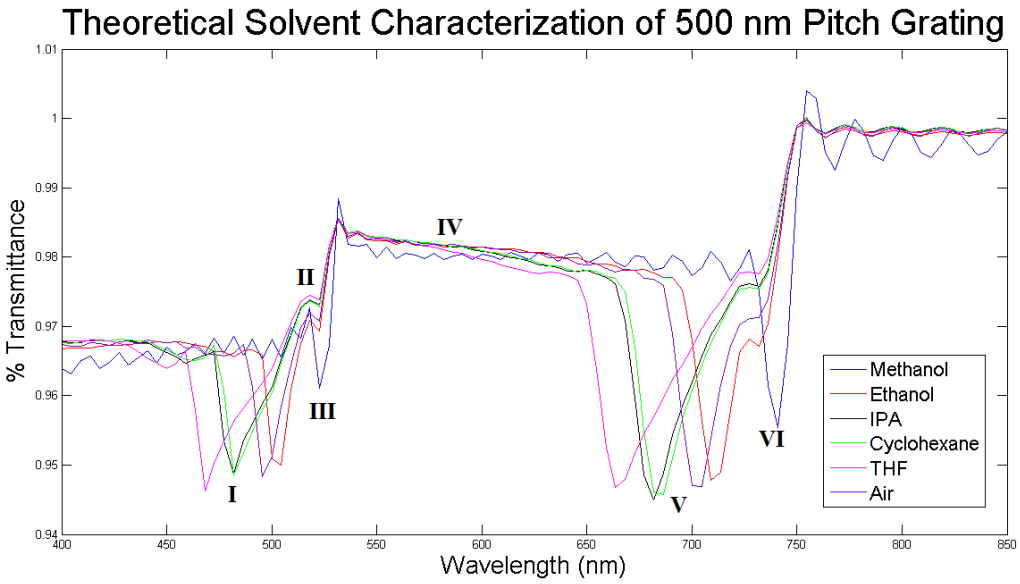

Figure 4.3: Comparison of theoretical spectral output of 500 nm pitch grating exposed to liquids of varying RI

The effect of thin deposited layer thickness(30m-100nm) on the spectra of the 500nm and 1μm gratings are displayed in figures 4.7 and 4.8, respectively. The effect of the thick deposited layers(200nm-1.5μm) on the spectra of the 1μm grating is shown in Figure 4.9. The relationship between the thick and thin layers was determined to be linear. The slope of this linear fit is the sensitivity of the grating to the deposited layer thickness.

The optimization study of the nanohole grating performed in Lumerical output the figure of merit shown in Figure 4.10. From this study it was determined that the optimal pitch would be 959nm.

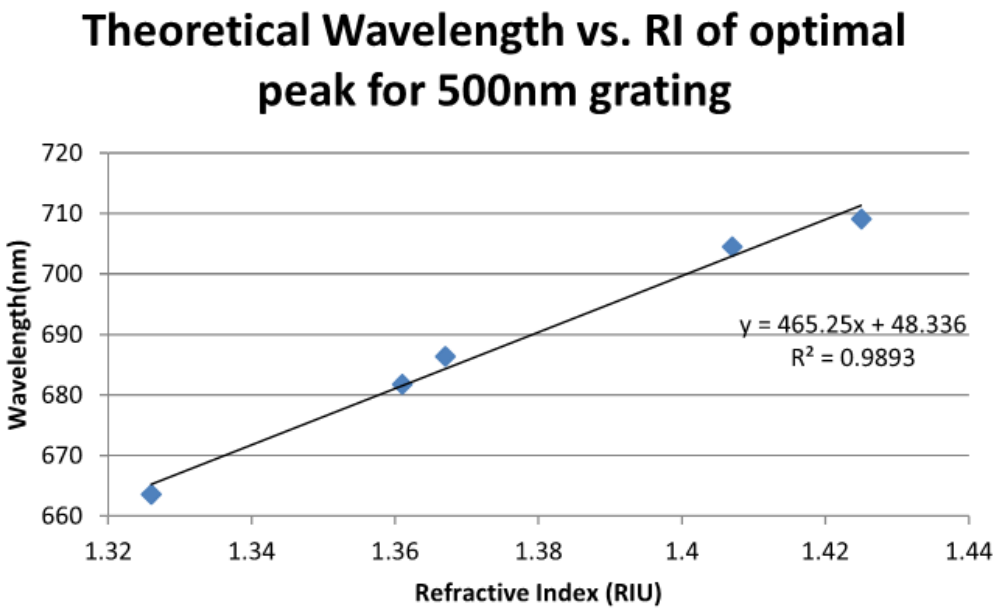

Figure 4.4: Determination of theoretical bulk sensitivity for 500 nm pitch grating

4.2 Origin of transmission spectra

The transmission spectral output of the nanohole arrays is dependent on many factors, and is therefore not straightforward. Figures 4.5 and 4.3 show the theoretical output spectra of the 1μm and 500nm pitch, respectively, in response to different solvents with varying refractive indices. The 500nm pitch grating will be used to discuss the origins of spectral features. However, the 1μm pitch is used to support some of the claims made for the origin of spectral features for the 500 nm grating. Each of the peaks in the 500 nm pitch transmission spectrum are classified by a roman numeral, which is how each peak will be referred to throughout this discussion.

The spectra of both the 1μm and 500nm pitch gratings exhibit a slight drop in transmission around 750nm(peak VI in the 500nm spectrum). According to literature, aluminum, the metallic material the gratings are imprinted on, has a well known absorption peak at 1.6eV due to conductivity.[38] This photon energy is related to the wavelength by equation 4.4,

$$E = \frac{hc}{\lambda} \tag{4.4}$$

where h is Plank's constant(4.13566733×10-15eVs), c is the speed of light(299792458 m/s), E is the energy of the photon (eV), and λ is the wavelength (nm). Because the aluminum is blocking the transmission of 750nm wavelength, every

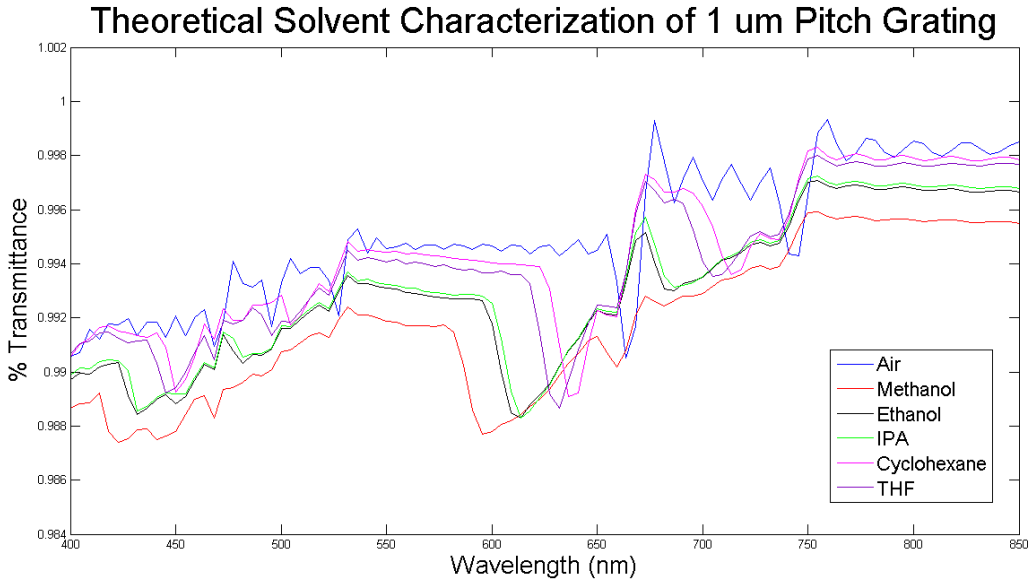

Figure 4.5: Comparison of theoretical spectral output of 1 μm pitch grating exposed to liquids of varying RI

grating fabricated with aluminum should exhibit this peak at relatively the same position and stay constant regardless of changing RI. This peak can be used as a calibration peak in an actual biosensing device.

Peak III, like Peak VI, does not shift in response to RI variation. However, this peak most likely originates from an SPP-BW predicted by equation 2.2.

Peak V arises from the coupling of a zero order RA at the top surface(n_{III}) with a zero order SPP-BW at the bottom surface(n_I). The order of this phenomena was determined from equations 2.2 and 2.1, where the RI at the bottom surface is known(n_I=1.5) and the free space incident wavelength that excites each phenomena is given by the wavelength at which the peak stays(550nm). Therefore, the position of this peak in response to varying region III dielectric materials can be predicted by equation 2.3. Thus this peak will also exhibit a sensitivity equivalent to the periodicity of the grating. It is important to note that the actual position of peak V is slightly red shifted compared to the position predicted by equation 2.3, which is due to the partial RA origin of the peak.

Peak I, like peak V, exhibits a wavelength shift in response to Ri variation. This peak is the result of the coupling of a (1,1) order RA and (1,1) order SPP-BW at the same surface between region I and II(n_I). This result can be

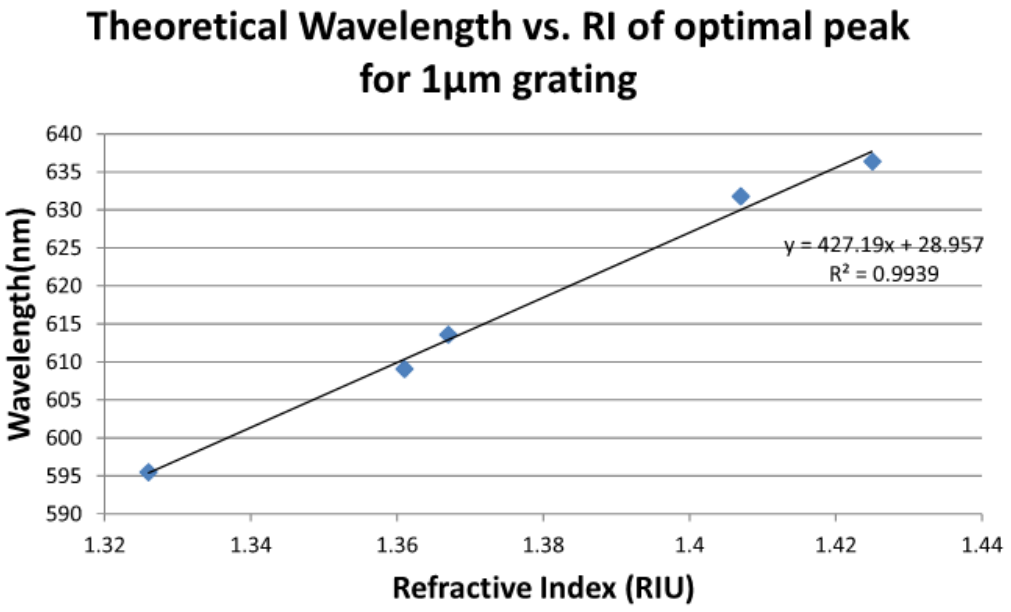

Figure 4.6: Determination of theoretical bulk sensitivity for 1 μm pitch grating

predicted by equations 2.2 and 2.1. Because these spectral features are first order, the sensitivity will not be equivalent to the periodicity.

Peaks II and IV are simply regions of constructive interference where no spectral features are causing a dip in transmission. Thus they are maxima arising from the presence of minima in the spectrum and are related to the general transmission through the nanoholes.

4.2.1 Hole Geometry

The geometry of the holes can have an effect on the position and transmission through the holes because any change in the holes will change the surface plasmons that will be excited by incoming light. Moreno et.al examined the sensitivity of the transmission spectrum to nonuniformities in the hole area in order to explain minor inconsistencies between their theoretical and experimental results. They confirmed that changes in the geometry of the holes accounted for the small variations in transmission efficiency and peak positions between thier theoretical and experimental results.[39]

In another study, Koerkamp et.al observed the effect of hole shape on the transmission spectra of nanohole arrays and found that using rectangular shaped holes enhanced transmission and caused a red shift in the spectrum.[40] In a later study, Molen et.al demonstrated that there are localized modes in-

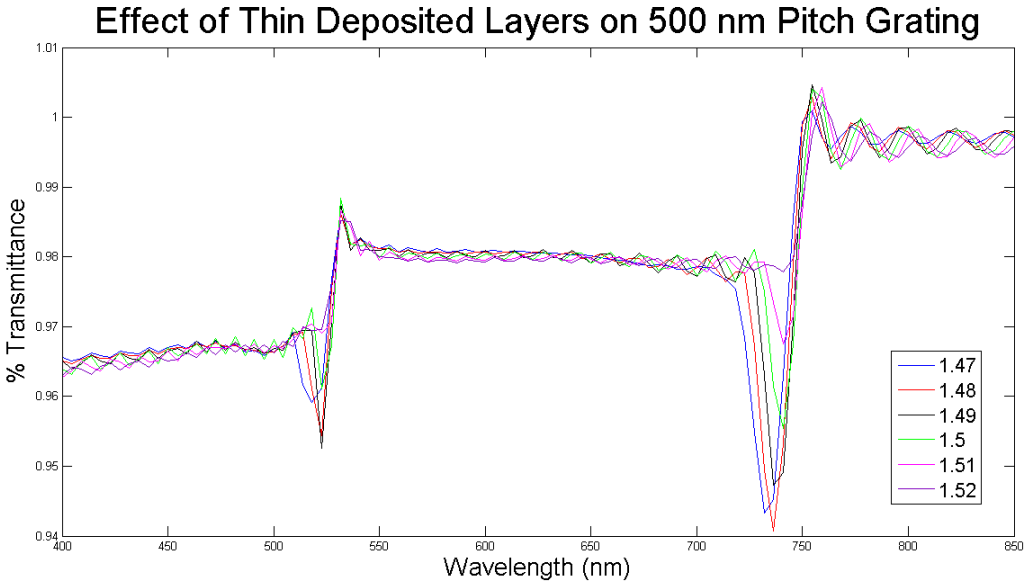

Figure 4.7: Theoretical deposited layer thickness effect(<100 nm) of the 500 nm pitch grating

side the rectangular holes arising from additional shape resonances that are not present in circular holes. These localized modes effectively acted as waveguides increasing the coupling efficiency of surface plasmons between both sides of the film and gave rise to further enhanced transmission and slight red shifts in the spectrm.[41] Thus, irregularities in the size and shape of the holes can effect the spectral output of the nanohole arrays.

4.3 Coupling Light into a waveguide

The RI mismatch between a high RI guiding layer surrounded by materials with lower refractive indices in an optical waveguide causes total internal reflection(TIR) of light. When light is coupled into this guiding layer, the majority of that light is successfully trapped inside the waveguide so that it can propagate over long distances. However, some of the light extends into the substrate and medium in the form of an electromagnetic wave, called the evanescent field, which experiences an exponential decay in amplitude as it moves away from the surface. The angle of incident light is changed to match the evanescent wave propagation rate with the propagation rate of the SPPs.[42] Thus the field extends into the recognition substrate and sample medium thereby enhancing the sensitivity of molecule recognition because of the large difference between

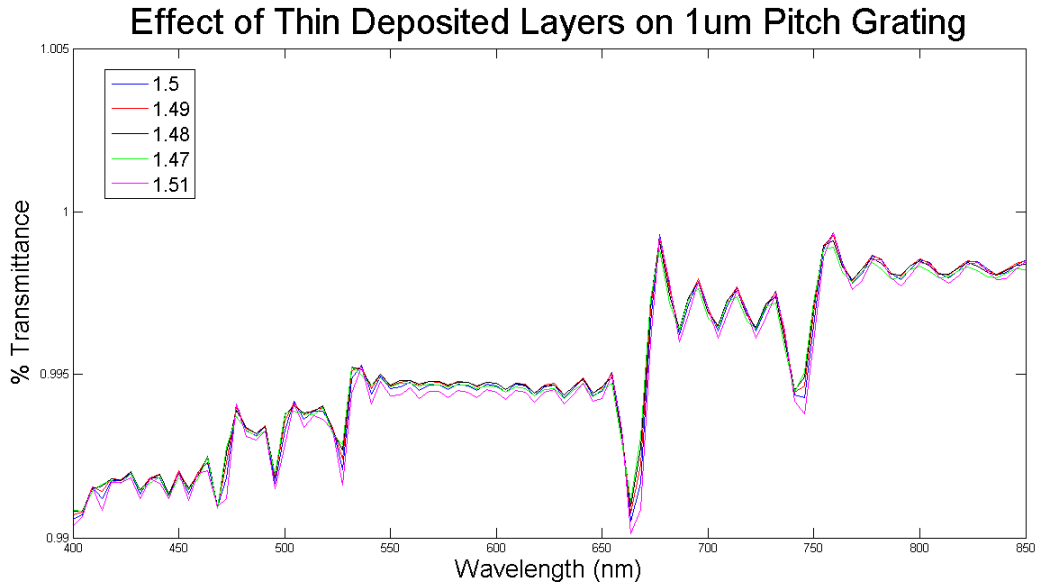

Figure 4.8: Theoretical deposited layer thickness effect(<100 nm) of the 1 μm pitch grating

the analytes attached to the surface and the other molecules present in the sample.[43]

Nanohole arrays can act as grating couplers to excite the guided mode in a planar waveguide. Because SPPs are tightly bound to the surface were they originate, they will not excite the guided mode in a waveguide without energy from an external light source. When the frequency and angle of incident light matches the resonance conditions to excite an SPP, the incident light constructively interferes with the SPP and propagates into the waveguide. However, when the light hitting the grating does not match the resonance conditions to excite an SPP, the light will behave almost the same as it would if it was incident in an area where there is no grating.[44] Therefore, SPPs arising from nanohole arrays that match the resonance conditions of the guided mode in a planar waveguide can couple light into that waveguide.

4.4 Chapter Summary

This chapter explained the basics of FDTD simulations and presented the results of the theoretical characterization and optimization of the nanohole array as a RI sensor. The bulk sensitivities and deposited layer thickness effects of the 500 nm and 1 μm gratings were illustrated. The origins of the transmission spectra were discussed as well as the potential of the device to

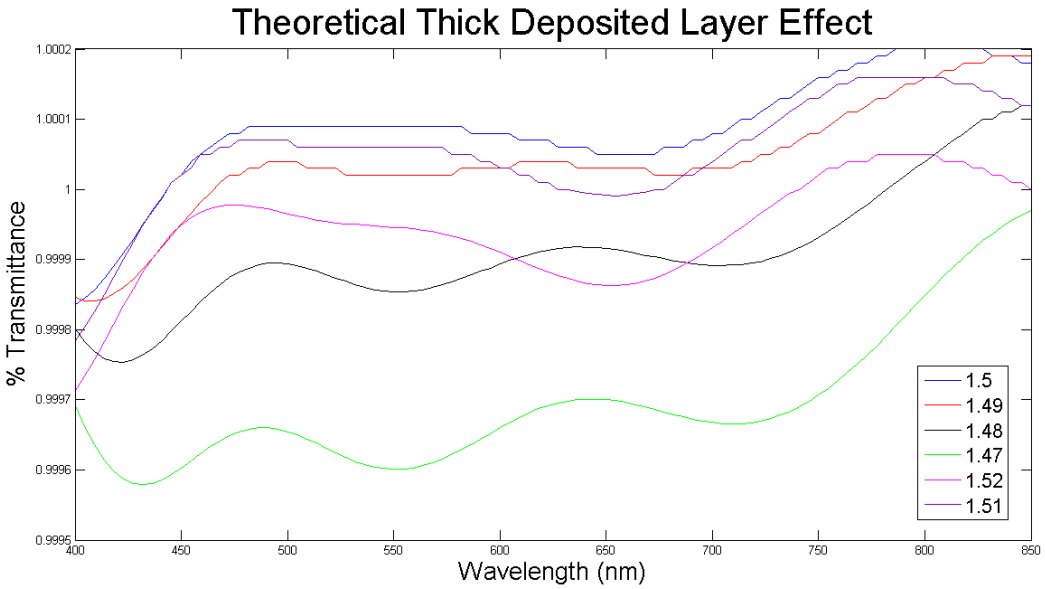

Figure 4.9: Theoretical deposited layer thickness effect(>200 μm) of the 1 μm pitch grating

couple light into a waveguide. The experimental characterization results are presented in the next chapter.

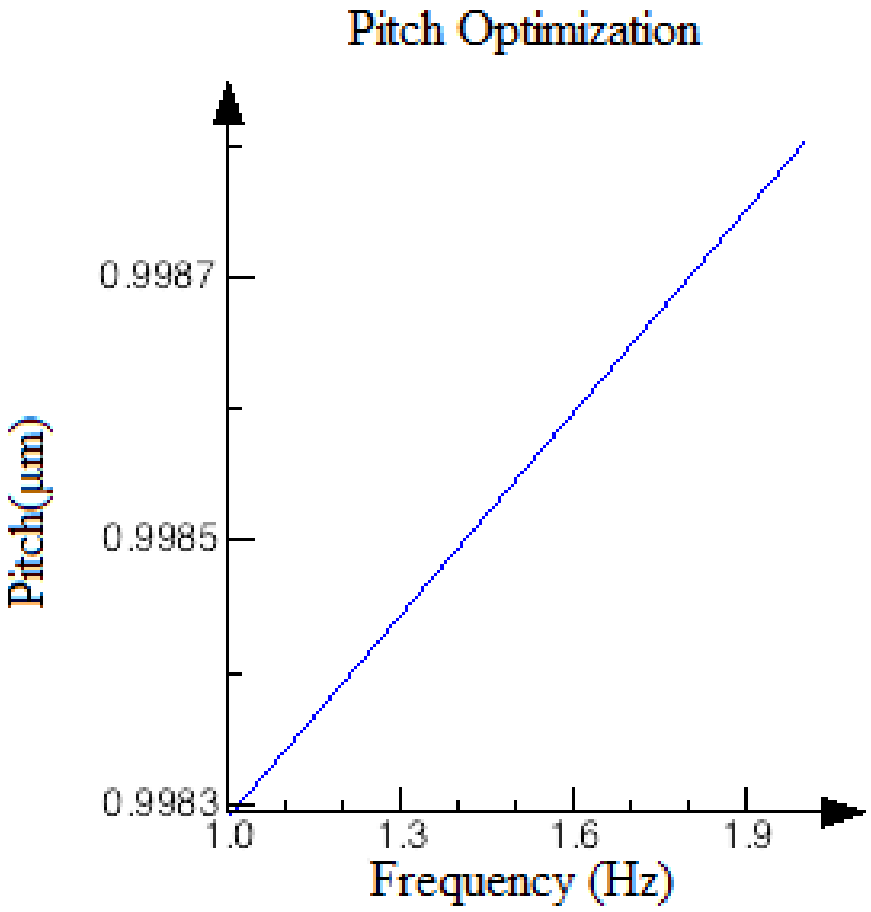

Figure 4.10: Figure of Merit from the Lumerical pitch optimization simulation which demonstrates the pitch that gives the sharpest transmission spectrum.

Chapter 5

Experimental Results

5.1 Solvent Characterization Results

The 1μm grating spectral response is shown in Figure 5.1. The optimal peak was determined to be the one at 614nm when immersed in methanol, which fluctuates in the wavelength range from 550nm to 650nm. This optimal peak was used for solvent characterization. The relationship between the refractive index and wavelength shift for the optimal peak of the 1μm grating is given in Figure 5.2. There was a linear trend between the refractive index and wavelength which is displayed in that figure. The R^2 value for the linear fit line is 0.9925, which demonstrates the accuracy of this fit. The bulk sensitivity was determined from the slope of this graph and was 409nm/RIU.

The 500nm grating spectral response is shown in Figure 5.3. The optimal peak used for solvent characterization is located at 671nm when immersed in methanol, which stays in the wavelength range from 650nm to 750nm. The relationship between the refractive index and wavelength shift for the optimal peak of the 500nm grating along with the linear trend equation is given in Figure 5.4. The R^2 value for this grating is 0.9561, which is an acceptable fit for the data. The bulk sensitivity of this grating was found to be 532nm/RIU.

5.2 Thickness Sensitivity

Deposited films with varying thicknesses had varying effects on the peaks in the transmission spectra of the nanohole grating samples. The spectral response of the 500nm pitch grating to varying deposited film thicknesses is shown in Figure 5.5. It is apparent that certain peaks, like the optimal peak

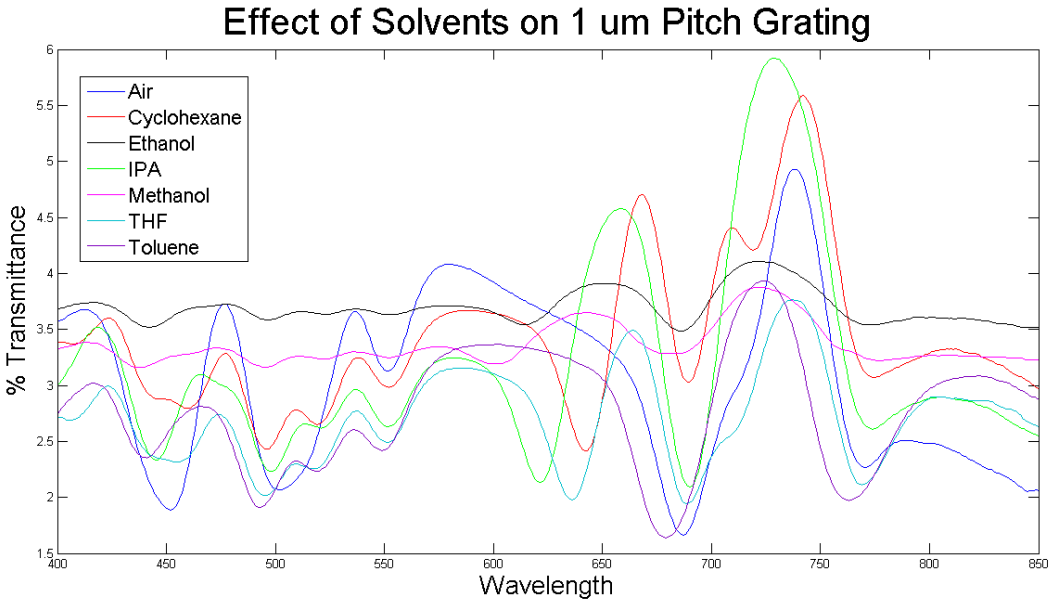

Figure 5.1: Comparison of spectral output of 1μm pitch grating exposed to liquids of varying refractive index

used for characterization, exhibit large shifts in response to the deposited layer thickness variance, while other peaks like the one at 750nm stays almost completely constant. Figure 5.6 shows the relationship between wavelength shift and deposited layer thickness for the 500nm peak of the 500nm pitch grating.

Figure 5.7 demonstrates the spectral shift of the optimal peak of the 1μm pitch grating in response to varying deposited film thicknesses between 200nm and 1.5μm. Like the 500nm pitch grating sample, there are large shifts in certain peaks of the 1μm output spectrum in response to thickness variation, like the optimal peak, but little to no shift in others, like the one around 700nm. There is a large contrast between the effect of thick deposited layers on the grating output spectrum and the effect of thinner deposited layers, between 20nm and 100nm, on the output spectrum as shown in Figure 5.8. This difference is much more apparent in the graphs of wavelength vs. thickness for the thick and thin layer experiments, shown in figures 5.9 and 5.10, respectively. There is a linear trend between thickness and wavelength for thin layers, but there is a much more complicated polynomial relation between the variables when the deposited layers are thick(>200nm).

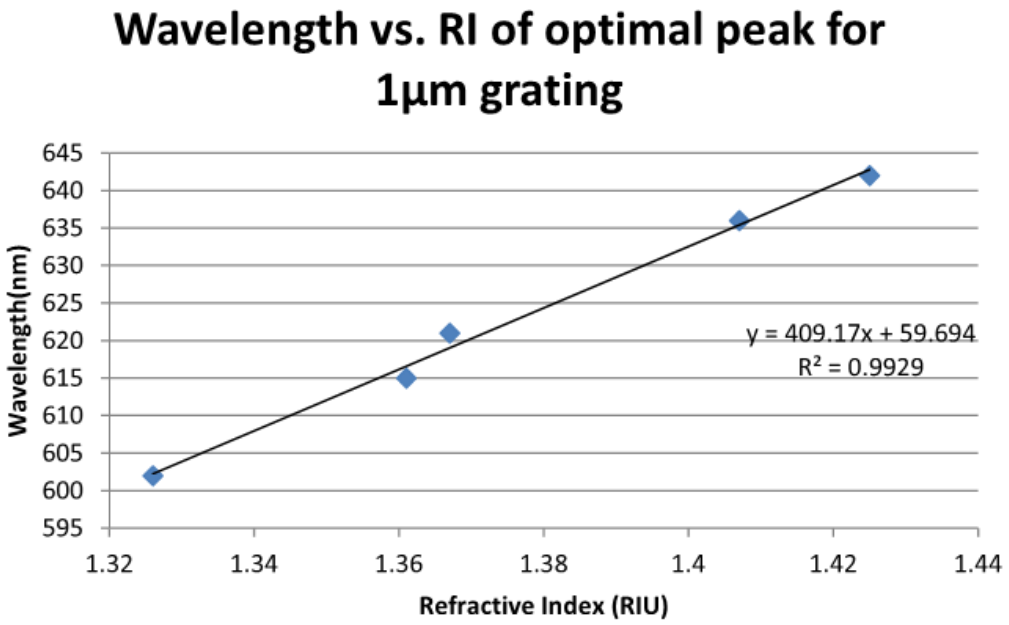

Figure 5.2: Determination of Bulk Sensitivity for 1μm pitch grating

5.3 Polarization

The effect of exposing the grating to different polarizations of light is shown in Figure 5.11. There is some variation in transmission but not in the position of the peaks.

5.4 Biomolecule detection

The effect of biomolecule recognition on the transmission spectrum of a 500nm pitch nanohole grating sample was very pronounced. Figure 5.12 demonstrates the effect of each step of the functionalization and recognition processes on the spectral output of the gratings. From this graph it was determined that there was a 22nm wavelength shift towards the red part of the spectrum in the peak around 550nm from the original nanohole array to the final sample with recognized molecules on the top. However, there is only a 10nm red shift of the spectrum in the peak around 550nm in response to MCLR antibodies binding to the MCLR molecules immobilized on the surface of the samples. Selective molecule recognition was confirmed at UPM ISOM by using the bare glass comparison procedures explained by Herranz et.al.[31]

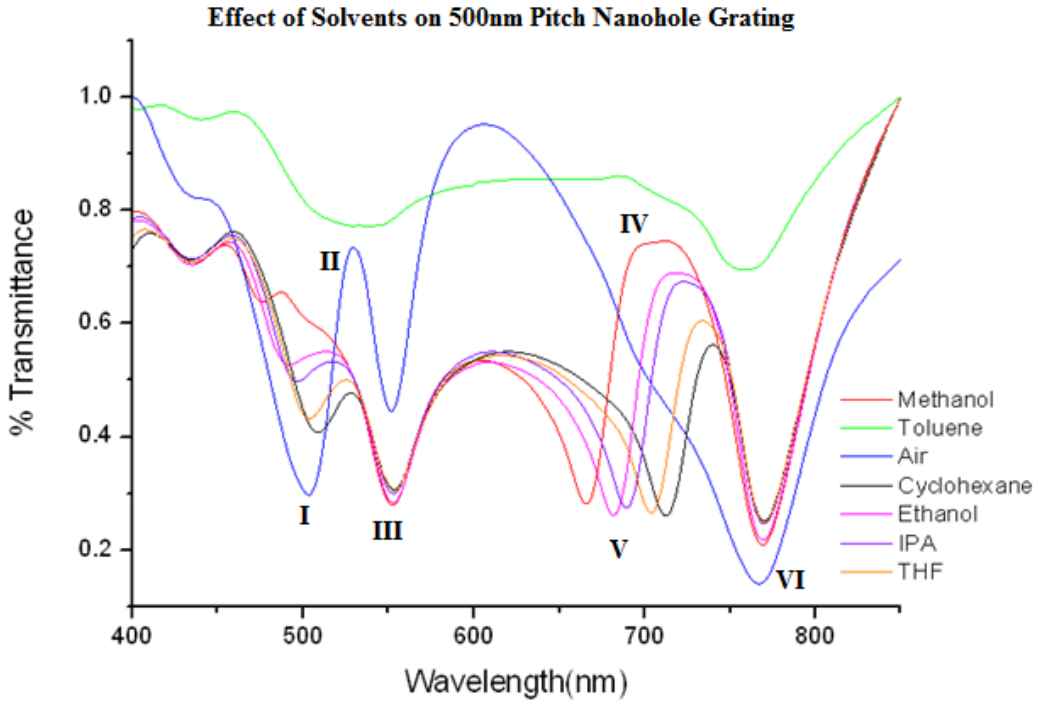

Figure 5.3: Comparison of spectral output of 500nm pitch grating exposed to liquids of varying refractive index

5.5 MIP Molecule Detection

Fluorescent images of the samples including MIP layers were taken before the template molecules were removed from the polymerized polymer, after template molecule removal, after incubation, then after a second washing step and those images are shown in figures 5.13, 5.14, 5.15, and 5.16, respectively. A NIP was prepared at the same conditions and put through the same tests as the MIP, but showed no traces of analyte presence at any point. Figure 5.17 shows a fluorescent microscope capture of the NIP after incubation, demonstrating that there was no analyte recognition by the NIP. Images of the NIP were taken throughout the different steps, but the NIP stayed constant without recognition throughout all the experiments, so only one image is presented here.

5.6 Chapter Summary

The results of the experimental charactertization were presented in this chapter. The bulk sensitivities and deposited layer thickness effects of the

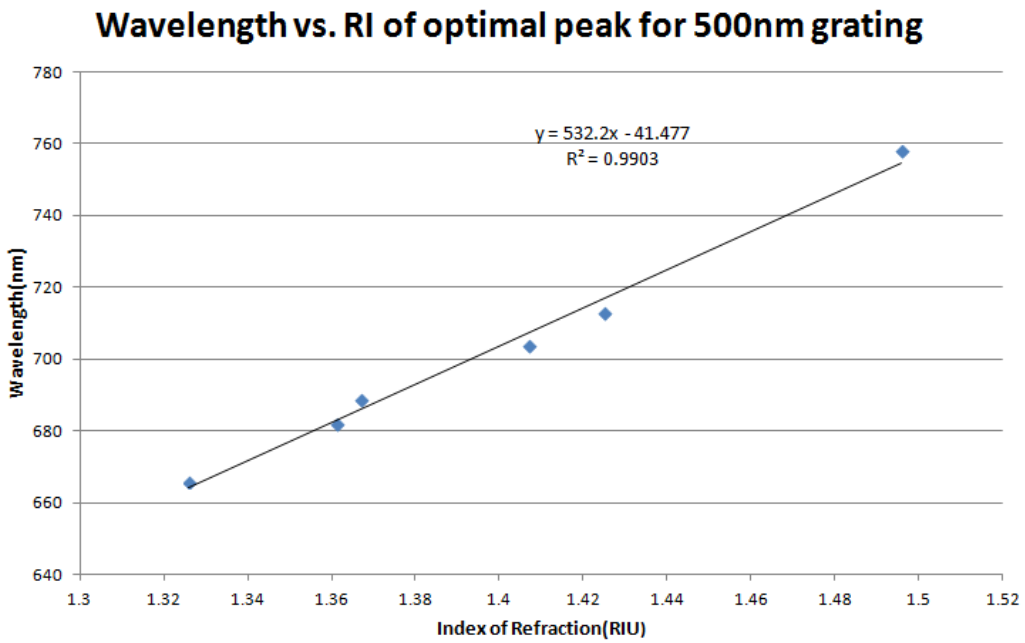

Figure 5.4: Determination of Bulk Sensitivity for 500nm pitch grating

fabricated 500 nm and 1 μm pitch nanohole arrays were illustrated. The results of the biomolecule and MIP recognition experiments were also displayed. The significance of these results and comparsion to the theoretical results presented in the last chapater will be discussed in the next chapter.

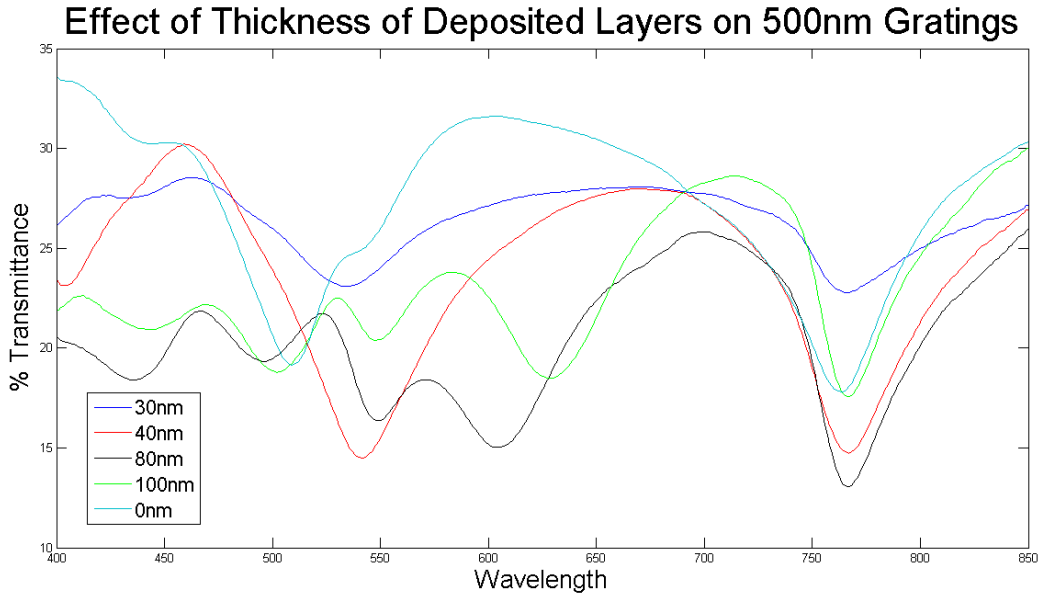

Figure 5.5: Effect of deposited layer thickness on the transmission spectrum of the 500nm pitch nanohole grating sample for layer thicknesses smaller than 100 nm

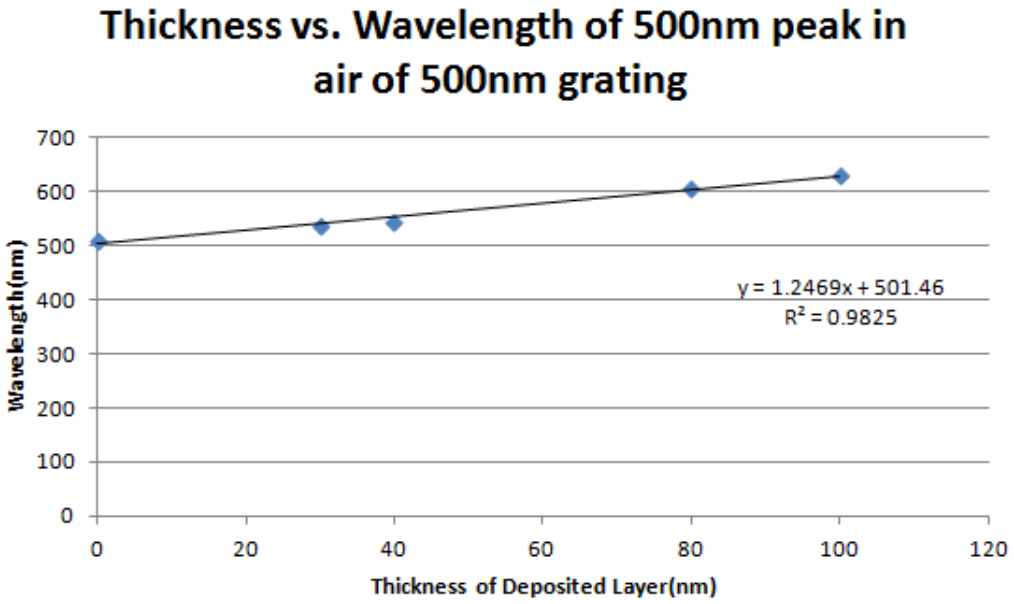

Figure 5.6: Effect of deposited layer thickness on the transmission spectrum of the 500nm pitch nanohole grating sample

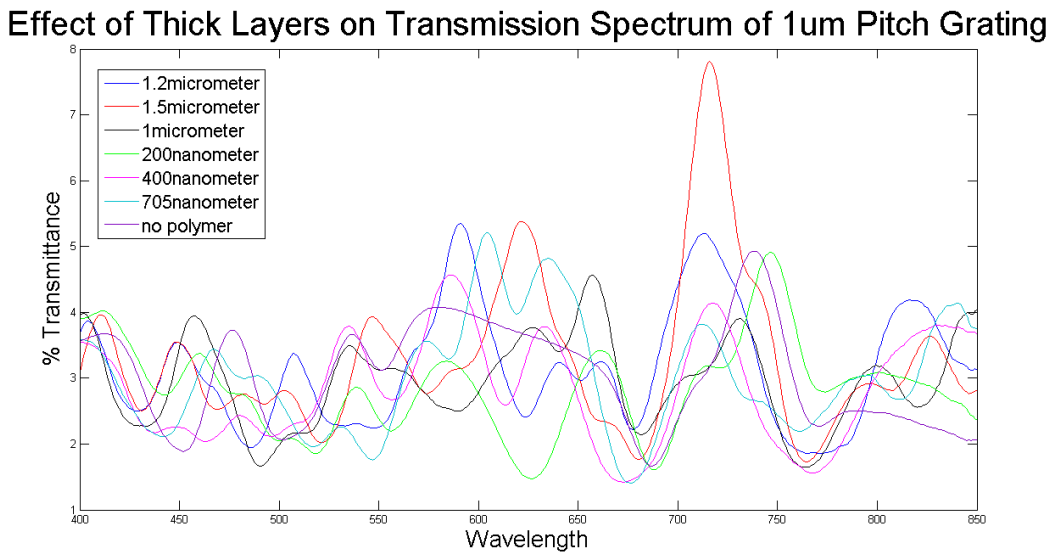

Figure 5.7: Effect of deposited layer thickness, between 200nm and 1.5μm, on the output spectrum of the 1μm pitch nanohole grating sample

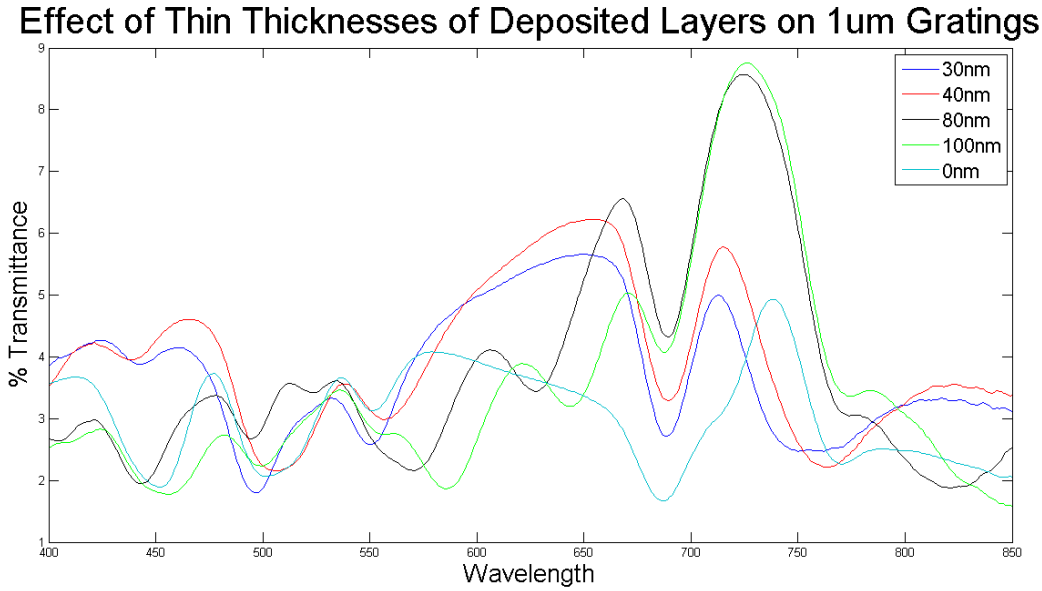

Figure 5.8: Effect of deposited layer thickness, between 20nm and 100nm, on the output spectrum of the 1μm pitch nanohole grating sample

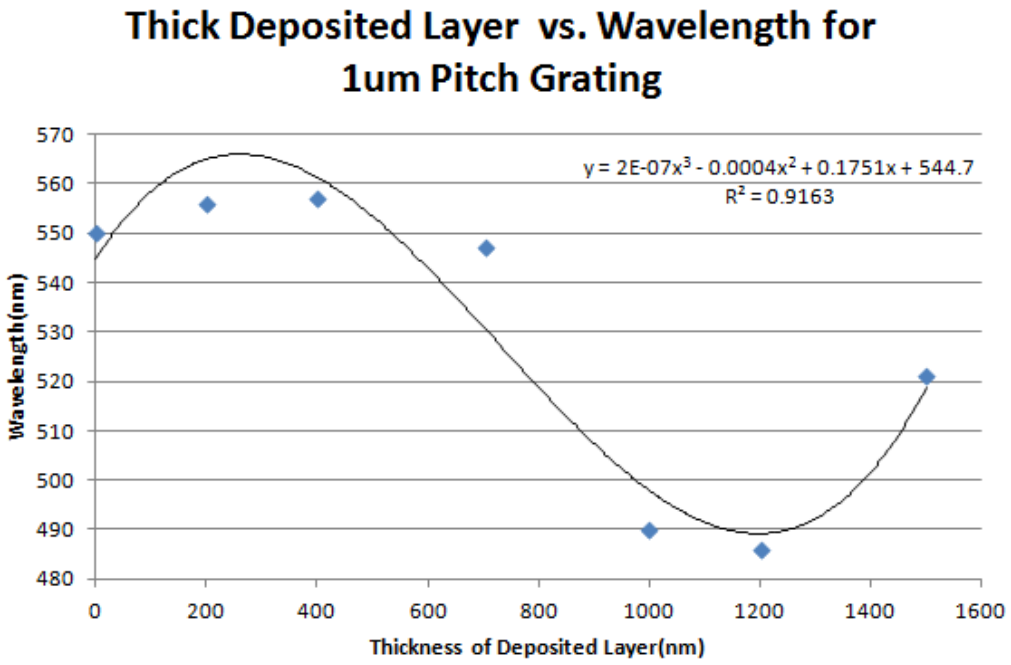

Figure 5.9: Relationship between deposited layer thickness, between 200nm and 1.5μm, and wavelength of the 1μm pitch nanohole grating sample

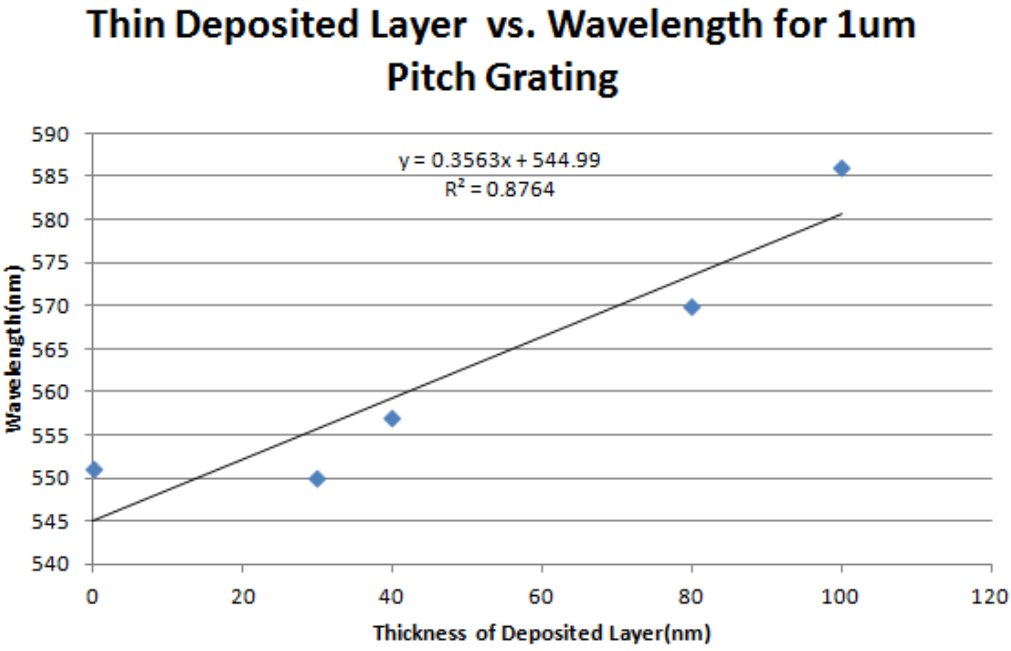

Figure 5.10: Relationship between deposited layer thickness, between 20nm and 100nm, and wavelength of the 1μm pitch nanohole grating sample

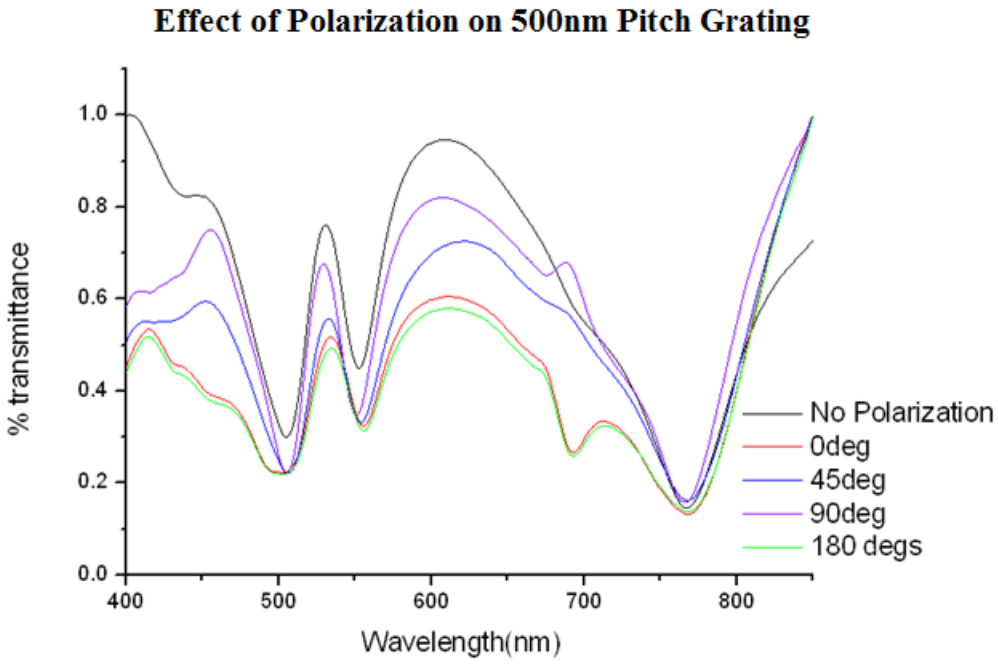

Figure 5.11: Effect of polarizing incoming light on the transmission spectrum of the 500nm grating.

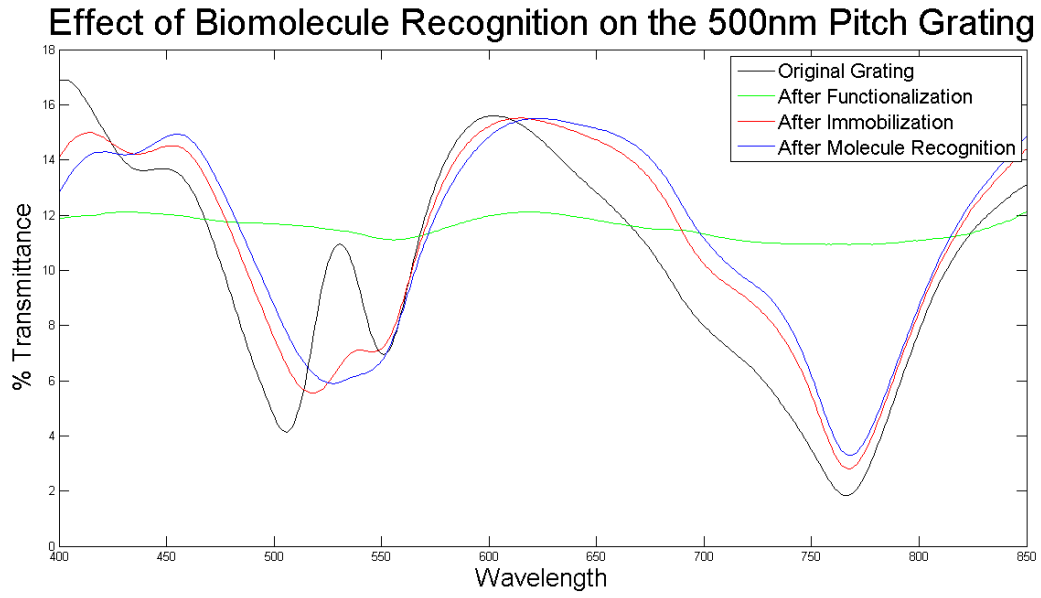

Figure 5.12: Comparison of the transmission spectra of a 500nm pitch grating during the steps of biomolecule recognition, which include functionalization of the metallic surface of the sample, immobilization of MCLR molecules onto that surface, and attachment of MCLR antibodies when exposed to an incubation solution

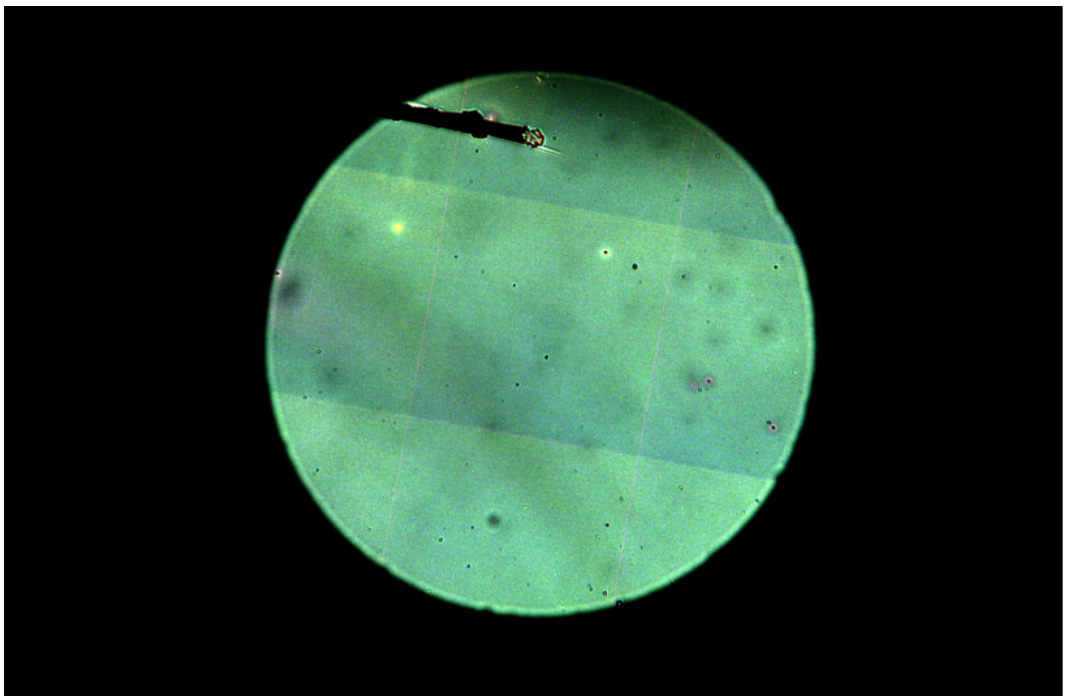

Figure 5.13: Fluorescent microscope image of original MIP layer including template molecules

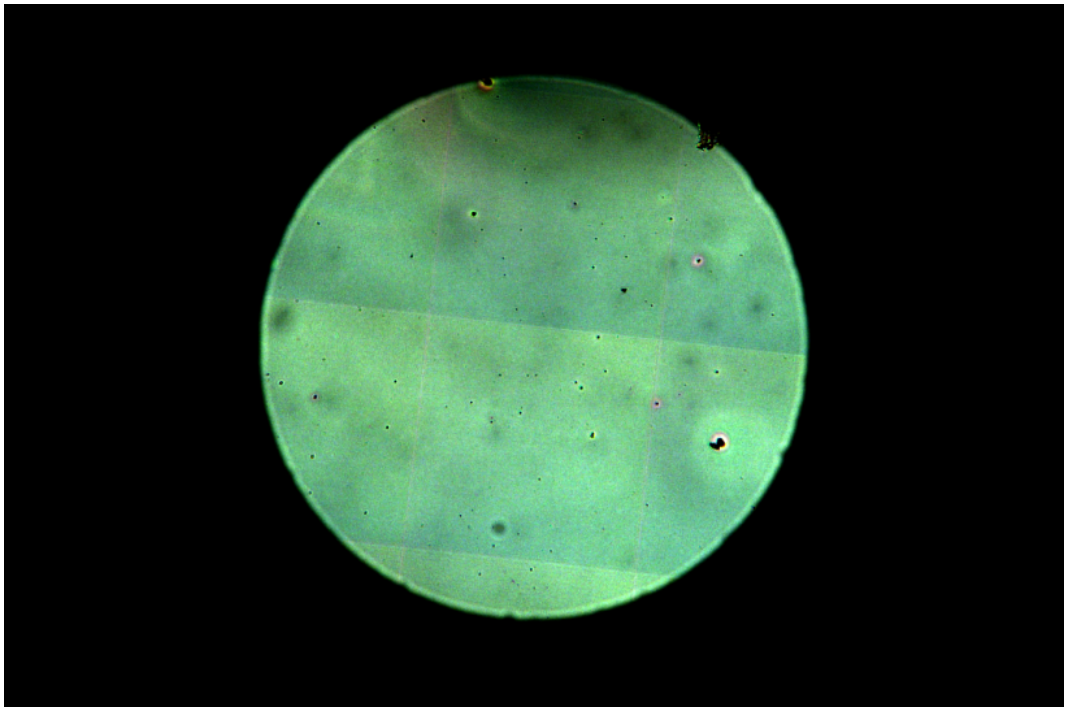

Figure 5.14: Fluorescent microscope image of MIP layer after template molecule are removed

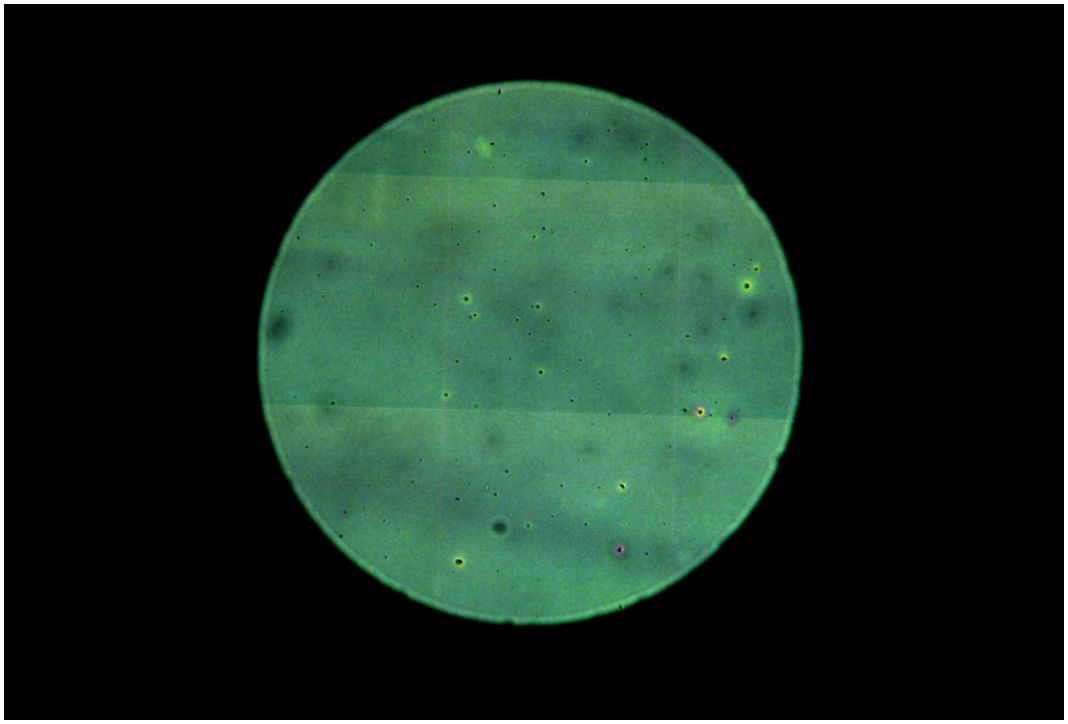

Figure 5.15: Fluorescent microscope image of MIP layer after incubation in a 30μg/L Rhodamine 123 solution overnight

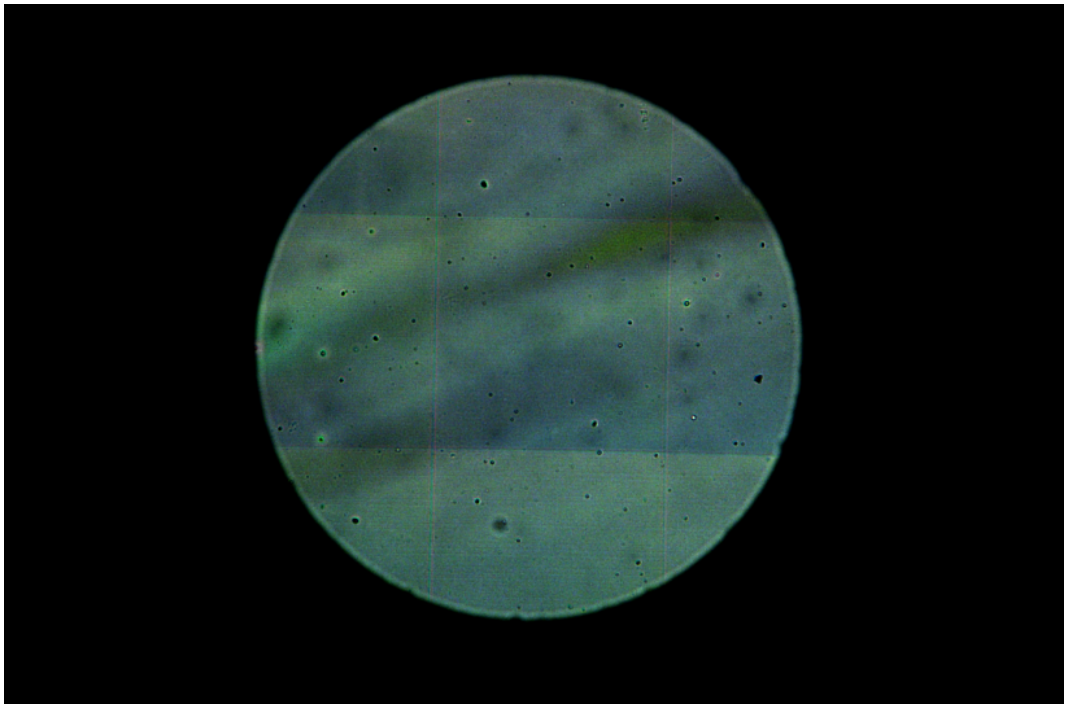

Figure 5.16: Fluorescent microscope image of MIP layer after wash step to remove any recognized Rhodamine 123 molecules

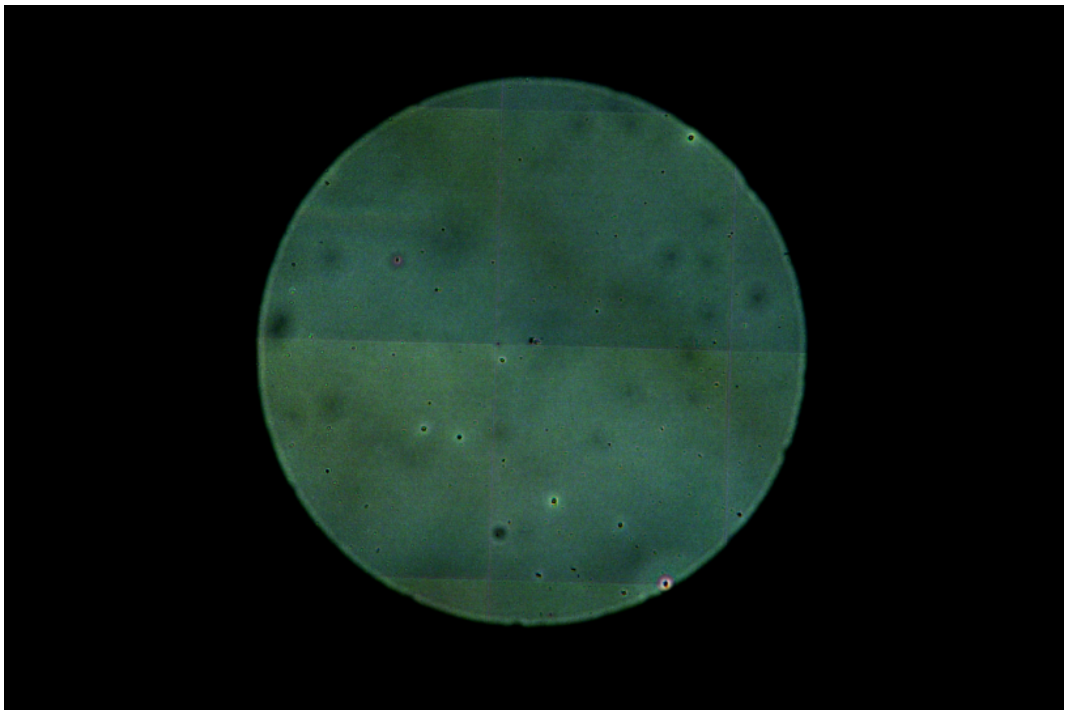

Figure 5.17: Fluorescent microscope image of NIP layer, representing all images taken throughout the process of washing and incubating.

Chapter 6

Discussion

6.1 Solvent Characterization

The theoretical transmission spectrum responding to solvents with varying refractive indices (Figure 4.3) had much sharper peaks than the experimental spectral output(Figure 5.3) for the 500 nm pitch grating, which is the result of variations in the geometry of the holes. The experimental output also had extra peaks arising from additional interference between unexpected excitations of surface plasmons, which most likely resulted from variations in the hole shape. Figure 3.2 shows an SEM picture of the nanohole arrays in which it is noticed that that some of the shapes are elliptical and start to resemble rectangular structures. According to the theory, shape resonances may be arising from this more rectangular shape which could give rise to the additional peaks in the experimental spectrum. This could also be the reason that the bulk sensitivity of the 500 nm experimental nanohole array (532 nm/RIU) was higher than theoretical expectations (465 nm/RIU).

The nearly linear trend seen in the experimental and theoretical bulk sensitivity determinations based on Peak I can be explained by equation 2.4. The experimental and theoretically determined graphs of wavelength as functions of surface refractive index variance is very similar to the zero order positions of RAs as a function of RI variance in region III. Furthermore, the slopes of these graphs, which represent the bulk sensitivity, were very close to the periodicity of the grating (500 nm) because they are due to RA-SPP phenomenon. Peak III can be explained in the same way, but the bulk sensitivity(315 nm/RIU) calculated for this pitch is not as close to the pitch of the grating and has more variation in the linear trend. These variations are most likely due to an inexact matching of the RA and SPP-BW. Peak III is much broader than peak I and

does not occur when the region III medium is air or toluene, which suggests that the incoming beam of light only matches the resonance of SPPs at this wavelength in a limited RI range. Therefore this spectral feature was not used as the characterization peak of the device for refractive index sensing.

The nanohole arrays imprinted in aluminum showed similar bulk sensitivity(532 nm/RIU) to nanohole arrays imprinted in silver(450 nm/RIU) and gold(500nm/RIU), despite these noble metals being a better-performance plasmonic materials.[4,7] These results have demonstrated that aluminum, a much cheaper metal, can replace more expensive plasmonic materials like silver and gold as the metallic materials for sub-wavelength hole arrays.

Polarization of the incoming light to the nanohole array did not have a large effect on the position of the peaks in the transmission spectrum, but have an effect on the percent of light transmitted. The nanohole array can theoretically be optimized by choosing a polarization of light that will maximize transmission, however in this case, unpolarized light had the highest transmission.

6.2 Deposited Layer Thickness

The Filmetrics measurements on the experimental films with deposited polymer layers of varying thickness confirmed that there were slight variations in refractive index(between 1.48 and 1.52) caused by scattering through the deposited layer. Thus the theoretical layer thickness simulations were performed in refractive index increments of 0.01, which represent the refractive index change caused by varying thickness. The experimental results showed a linear trend between wavelength and deposited layer thickness in the 1 μm pitch grating for layers less than 100 nm but a third order polynomial relationship for between the two for layer thicknesses greater than 200 nm. Similar results were observed for the theoretical simulations, which supports the theory that the nanoholes were completely filled when the deposited layer was thicker than 200nm but either unfilled or partially filled for layer thicknesses less than 100 nm.

The 500 nm thickness experiments and theoretical simulations confirmed that there is a linear trend between wavelength and deposited layer thickness for layers less than 100 nm. There is a much less prominent effect on the transmission when the nanoholes are not compeletely filled by the deposited

polymer layer, which occurs when the layers are less than 100 nm. Therefore the ideal MIP recogntion layer should be less than 100 nm thick.

6.3 Biosensing Capabilities

The biomolecule detection experiment demonstrated the ability of the nanohole array to act as a transducer for label-free optical biosensing. The transmission spectrum showed detectable shifts in response to the binding of analyte molecules to the immobilized biomolecule on the surface of the nanohole array as depicted in Figure 5.12. However, each step of the biomolecule recognition experiment produced a slight red shift, which must be taken into consideration when calculating the concentration of bound analyte in an actual biosensing device. The device must be calibrated so the wavelength shift is calculated between final immobilization of molecules on the surface and analyte recognition instead of between the original grating and analyte recognition.

A novel polymer was used to create the MIP recognition layer in order to demonstrate the potential of combining the nanohole array and MIP technologies to further the advantages of the technology. Fluorescent microscopy confirmed that the polymer-Rhodamine 123 layer before the Rhodamine 123 template molecules were removed contained the template molecules(Figure 5.13), and that the template molecules were fully removed after washing (Figure 5.14). Although more difficult to see, there was slight recognition achieved by the MIP layer after incubation (Figure 5.15). The recognized molecules were again removed by a second washing step(Figure 5.16), thus demonstrating the reusability of the MIP. A NIP was used as a control to prove that the fluorescence seen in each step of the MIP was truly due to recognition(Figure 5.17).

Because the polymer used to make the MIP is previously uncharacterized, it was not optimized for this study and thus these results are not a complete realization of the full potential of the MIP as a synthetic recognition element. The absorption peak of Rhodamine 123 corresponds to a transmission dip around 500 nm and the 500 nm pitch grating had a transmission dip at nearly the same location. Therefore it was difficult to determine if there was any change in the transmission spectrum due to the presence or absence of molecules. Therefore, biomolecule recognition by the MIP was impossible to determine purely from transmission. When designing and optimizing a biosensor, the position

of the peaks and dips of the spectrum must be considered in relation to any transmission effects caused by the analyte .

6.4 Chapter Summary

In this chapter, the theoretical and experimental characterization results were compared and the meaning of the difference between them was discussed. The biosensing capabilities of the device were also evaluated.

Chapter 7

Conclusions

This thesis has characterized a periodic nanohole array as a transduction element in a biosensor. Transmission spectroscopy was used to monitor the response of the nanohole array to refractive index changes arising from exposure to different solvents, varying deposited polymer layer thicknesses, and binding events between biological or synthetic recognition elements and analytes in a sample solution. Theoretical simulations were performed to support experimental results and optimize the pitch of the gratings for use in a biosensor. The ability of the nanohole array to couple light into a waveguide was discussed to demonstrate the potential of the nanohole array to be incorporated into integrated biosensing devices.

It has been demonstrated that aluminum has plasmonic sensing capabilities, making it a much cheaper alternative to traditional thin film substrate materials like gold and silver. Thus, nanohole arrays incorporating this more cost effective material can facilitate widespread applications of metallic nanohole arrays for biosensing technologies. In addition, a novel polymer has been used to make the MIP biomimetic recognition element and has showed signs of being a viable synthetic recognition element that can reduce the cost and increase the robustness of biosensors.

7.1 Future Work

There is much work to be done in order to create a fully functioning biosensing device. The ability of the sub-wavelength periodic structures imprinted in aluminum to couple light into a waveguide for a complete biosensing reader device have been discussed though the actual integration of the technologies was beyond the scope of thesis. Much future work is needed to create a viable

label-free integrated optical waveguide bio(mimetic) sensor incorporating the nanohole grating coupler and MIP as a recognition element. The novel MIP polymer must be characterized and optimized for recognition of analyte, stability under a variety of environmental conditions, reusability, and interaction with the nanohole refractive index grating sensor.

Further theoretical and experimental optimization of the nanohole arrays must be performed to ensure maximum sensitivity and repeatability of results. The effect of hole penetration into the aluminum substrate must be studied to fully understand and optimize the imprinting process. Furthermore, the optimal geometry of the holes should be studied to ensure maximum transmission and sensitivity . In order to successfully incorporate the nanohole array and MIP technologies, the extent of polymer filling the holes must be determined to fully understand the effect of the polymer layer on the transmission spectrum. Along the same lines, the extent of solvent filling the holes during measurements should be studied.

Bibliography

[1] Ahmet A. Yanik, Min Huang, Osami Kamohara, Alp Artar, Thomas W. Geisbert, John H. Connor, and Hatice Altug. An optofluidic nanoplasmonic biosensor for direct detection of live viruses from biological media. *Nano Letters*, 10(12):4962–4969, 2010.

[2] Matthew A. Cooper. Optical biosensors in drug discovery. *Nature Reviews Drug Discovery*, 1:515–528, July 2002.

[3] G.M. Hwang, Lin Pang, E.H. Mullen, and Y. Fainman. Plasmonic sensing of biological analytes through nanoholes. *Sensors Journal, IEEE*, 8(12):2074 –2079, dec. 2008.

[4] Hyungsoon Im, Si Hoon Lee, Nathan J. Wittenberg, Timothy W. Johnson, Nathan C. Lindquist, Prashant Nagpal, David J. Norris, and Sang-Hyun Oh. Template-stripped smooth ag nanohole arrays with silica shells for surface plasmon resonance biosensing. *ACS Nano*, 5(8):6244–6253, 2011.

[5] A.G. Brolo. Plasmonics for future biosensors. *Nature Photonics*, 6(11):709–713, 2012.

[6] Gabriela Cervantes Tellez, Aftab Ahmed, and Reuven Gordon. Optimizing the resolution of nanohole arrays in metal films for refractive-index sensing. *Applied Physics A: Materials Science Processing*, pages 1–6. 10.1007/s00339-012-7405-5.

[7] J.M. McMahon, J. Henzie, T.W. Odom, G.C. Schatz, S.K. Gray, et al. Tailoring the sensing capabilities of nanohole arrays in gold films with rayleigh anomaly-surface plasmon polaritons. *Opt. Express*, 15(26):18, 2007.

[8] Antoine Lesuffleur, Hyungsoon Im, Nathan C. Lindquist, Kwan Seop Lim, and Sang-Hyun Oh. Plasmonic nanohole arrays for real-time multiplex biosensing. pages 703504–703504–10, 2008.

[9] Karsten Haupt. Peer reviewed: Molecularly imprinted polymers: The next generation. *Analytical Chemistry*, 75(17):376 A–383 A, 2003.

[10] M. Yan and O. Ramström. *Molecularly imprinted materials: science and technology*. CRC, 2004.

[11] CA Barrios, C. Zhenhe, F. Navarro-Villoslada, D. López-Romero, and MC Moreno-Bondi. Molecularly imprinted polymer diffraction grating as label-free optical bio (mimetic) sensor. *Biosensors and Bioelectronics*, 26(5):2801–2804, 2011.

[12] D.R. Shankaran, K.V. Gobi, and N. Miura. Recent advancements in surface plasmon resonance immunosensors for detection of small molecules of biomedical, food and environmental interest. *Sensors and Actuators B: Chemical*, 121(1):158–177, 2007.

[13] Inc. R D Sytems. Technical information: Detection visualization of antibody binding, 2012.

[14] V. Espina, E.C. Woodhouse, J. Wulfkuhle, H.D. Asmussen, E.F. Petricoin III, and L.A. Liotta. Protein microarray detection strategies: focus on direct detection technologies. *Journal of immunological methods*, 290(1-2):121–133, 2004.

[15] B.B. Haab. Methods and applications of antibody microarrays in cancer research. *Proteomics*, 3(11):2116–2122, 2003.

[16] Y. Fuchiwaki and I. Kubo. Electrochemical sensor based on biomimetic recognition utilizing molecularly imprinted polymer receptor. 2010.

[17] M. Pohanka and P. Skladal. Electrochemical biosensors–principles and applications. *J Appl Biomed*, 6(2):57–64, 2008.

[18] R. Karlsson, P.S. Katsamba, H. Nordin, E. Pol, and D.G. Myszka. Analyzing a kinetic titration series using affinity biosensors. *Analytical biochemistry*, 349(1):136–147, 2006.

[19] E. Hecht. *Optics*. Addison-Wesley, 4th edition, 1998.

[20] F.M. Grimaldi. *Adnexis*. Bernia, 1665.

[21] T.W. Ebbesen, H.J. Lezec, H.F. Ghaemi, T. Thio, and P.A. Wolff. Extraordinary optical transmission through sub-wavelength hole arrays. *letters to Nature*, 391:667–669, 1998. 10.1038/35570.

[22] Myeong-Woo Kim, Teun-Teun Kim, Jae-Eun Kim, and Hae Yong Park. Surface plasmon polariton resonance and transmission enhancement of light through subwavelength slit arrays in metallic films. *Opt. Express*, 17(15):12315–12322, Jul 2009.

[23] E.G. Loewen and E. Popov. Diffraction gratings and applications (optical engineering, 58). 1997.

[24] C.H. Wilcox. Theory of bloch waves. *Journal d'analyse mathématique*, 33(1):146–167, 1978.

[25] H. Gao, JM McMahon, MH Lee, J. Henzie, SK Gray, GC Schatz, TW Odom, et al. Rayleigh anomaly-surface plasmon polariton resonances in palladium and gold subwavelength hole arrays. *Opt. Express*, 17(4):2334–2340, 2009.

[26] K.S. SreeHarsha. *Principles of Physical Vapor Deposition of Thin Films*. Elsevier, 2006.

[27] Ian M. White and Xudong Fan. On the performance quantification of resonant refractive index sensors. *Opt. Express*, 16(2):1020–1028, Jan 2008.

[28] F. Romanato, KH Lee, G. Ruffato, and CC Wong. The role of polarization on surface plasmon polariton excitation on metallic gratings in the conical mounting. *Applied Physics Letters*, 96(11):111103–111103, 2010.

[29] R. Jelinek. *Cellular and Biomolecular Recognition*. Wiley, 2009.

[30] A.E.G. Cass, T. Cass, and F.S. Ligler. *Immobilized Biomolecules in Analysis: A Practical Approach*. The Practical Approach Series. Oxford University Press, 1998.

[31] S. Herranz, M.D. Marazuela, and M.C. Moreno-Bondi. Automated portable array biosensor for multisample microcystin analysis in freshwater samples. *Biosensors and Bioelectronics*, 33(1):50 – 55, 2012.

[32] Samuel Guillon, Remi Lemaire, Ana Valvanuz Linares, Karsten Haupt, and Cedric Ayela. Single step patterning of molecularly imprinted polymers for large scale fabrication of microbiochips. *Lab Chip*, 9:2987–2991, 2009.

[33] B. Sellergren. *Molecularly Imprinted Polymers: Man-Made Mimics of Antibodies and Their Application in Analytical Chemistry.* Techniques and Instrumentation in Analytical Chemistry, V. 23. Elsevier Science Limited, 2001.

[34] Inc Filmetrics. Operations manual for the filmetrics f20 thin-film analyzer. Technical report, Filmetrics, Inc.

[35] W. Yu. *Parallel Finite-Difference Time-Domain Method.* Artech House Electromagnetic Analysis Series. Artech House, 2006.

[36] K. Yee. Numerical solution of initial boundary value problems involving maxwell's equations in isotropic media. *Antennas and Propagation, IEEE Transactions on*, 14(3):302–307, 1966.

[37] Inc. Lumerical. Fdtd solutions user guide, 2003.

[38] L. W. Bos and D. W. Lynch. Low-energy optical absorption peak in aluminum and al-mg alloys. *Phys. Rev. Lett.*, 25:156–158, Jul 1970.

[39] L. Martin-Moreno, FJ Garcia-Vidal, HJ Lezec, KM Pellerin, T. Thio, JB Pendry, and TW Ebbesen. Theory of extraordinary optical transmission through subwavelength hole arrays. *Physical review letters*, 86(6):1114–1117, 2001.

[40] K. J. Klein Koerkamp, S. Enoch, F. B. Segerink, N. F. van Hulst, and L. Kuipers. Strong influence of hole shape on extraordinary transmission through periodic arrays of subwavelength holes. *Phys. Rev. Lett.*, 92:183901, May 2004.

[41] K. L. van der Molen, K. J. Klein Koerkamp, S. Enoch, F. B. Segerink, N. F. van Hulst, and L. Kuipers. Role of shape and localized resonances in extraordinary transmission through periodic arrays of subwavelength holes: Experiment and theory. *Phys. Rev. B*, 72:045421, Jul 2005.

[42] Jir Homola. Present and future of surface plasmon resonance biosensors. *Analytical and Bioanalytical Chemistry*, 377:528–539, 2003. 10.1007/s00216-003-2101-0.

[43] H. Mukundan, A.S. Anderson, W.K. Grace, K.M. Grace, N. Hartman, J.S. Martinez, and B.I. Swanson. Waveguide-based biosensors for pathogen detection. *Sensors*, 9(7):5783–5809, 2009.

[44] J.N. Yih, Y.M. Chu, Y.C. Mao, W.H. Wang, F.C. Chien, C.Y. Lin, K.L. Lee, P.K. Wei, and S.J. Chen. Optical waveguide biosensors constructed with subwavelength gratings. *Applied optics*, 45(9):1938–1942, 2006.